Scler 19: 1367-1370, 2013.

10. Kimura T, Ishizawa K, Mitsufuji T, Abe T, Nakazato Y, Yoshida K, Sasaki A, Araki N. A clinicopathological and genetic study of sporadic diffuse leukoencephalopathy with spheroids: A report of two cases. ***Neuropathol Appl Neurobiol*** 39: 837-843, 2013.
11. Saitoh B, Yoshida K, Hayashi S, Yamasaki R, Sato S, Kamada T, Suzuki SO, Murai H, Iwaki T, Ikeda S, Kira J. Sporadic hereditary diffuse leukoencephalopathy with axonal spheroids showing numerous lesions with restricted diffusivity caused by a novel splice site mutation in the CSF1R gene. ***Clin Exp Neuroimmunol*** 4: 76-81, 2013.
12. Fujiwara Y, Mizuno T, Okuyama C, Nagakane Y, Watanabe-Hosomi A, Kondo M, Kuriyama N, Tokuda T, Matsushima S, Nishimura T, Nakagawa M. Simultaneous impairment of intracranial and peripheral artery vasoreactivity in CADASIL patients. Cerebrovasc Dis. 2012;33(2):128-34. doi: 10.1159/000334185.
13. Yamada K, Sakai K, Akazawa K, Sugimoto N, Nakagawa M, Mizuno T. Detection of early neuronal damage in CADASIL patients by q-space MR imaging. Neuroradiology. 2013 Feb;55(3):283-90. doi: 10.1007/s00234-012-1105-x. Epub 2012 Oct 25. PubMed
14. Watanabe-Hosomi A, Watanabe Y, Tanaka M, Nakagawa M, Mizuno T. Transendocytosis is impaired in CADASIL-mutant NOTCH3. Exp Neurol. 2012 Jan;233(1):303-11. doi: 10.1016/j.expneurol.2011.10.020.
15. Kinoshita M, Yoshida K, Oyanagi K, Hashimoto T, Ikeda S. Hereditary diffuse leukoencephalopathy with axonal spheroids caused by R782H mutation in CSF1R: case report. J Neurol Sci. 2012 Jul 15;318(1-2):115-8. doi:10.1016/j.jns.2012.03.012.

ARTICLE IN PRESS
YEXNR-10948; No. of pages: 9; 4C: 3, 7
Experimental Neurology xxx (2011) xxx–xxx
Contents lists available at SciVerse ScienceDirect
Experimental Neurology
journal homepage: www.elsevier.com/locate/yexnr

Regular Article

Transendocytosis is impaired in CADASIL-mutant NOTCH3

Akiko Watanabe-Hosomi [a], Yoshihisa Watanabe [b], Masaki Tanaka [b], Masanori Nakagawa [a], Toshiki Mizuno [a,*]

[a] Department of Neurology, Graduate School of Medical Science, Kyoto Prefectural University of Medicine, Japan
[b] Department of Basic Geriatrics, Graduate School of Medical Science, Kyoto Prefectural University of Medicine, Japan

ARTICLE INFO

Article history:
Received 11 July 2011
Revised 7 October 2011
Accepted 23 October 2011
Available online xxxx

Keywords:
CADASIL
NOTCH3
Endocytosis
Transendocytosis

ABSTRACT

Mutations in the human NOTCH3 gene cause cerebral autosomal dominant arteriopathy with subcortical infarcts and leukoencephalopathy (CADASIL), but the pathogenesis of CADASIL has remained unclear. Recently, endocytosis of the Notch ectodermal domain into ligand-expressing cells, called transendocytosis, has come to be considered critical for Notch activation. We hypothesized that the mutant NOTCH3 protein, particularly the ectodermal domain of NOTCH3 (N3ECD), may be refractory to degradation on the cell surface due to impaired transendocytosis. We established a co-culture system in which HEK293 cells stably expressing one copy of tetracycline-regulated NOTCH3 were cultured with NOTCH3 ligand Jagged1 (Jag1)-expressing HEK293 cells. We obtained three main results: first, the C185R mutant N3ECD on the cell surface was degraded significantly more slowly than the wild N3ECD when NOTCH3 cells were co-cultured with Jag1-expressing cells. Second, both the wild-type and mutant NOTCH3-expressing cells increased HES1 expression on co-culture with ligand-expressing cells. Third, vesicles containing N3ECD were observed in Jag1-expressing cells. Vesicles of mutant N3ECD within the Jag1-expressing cells were significantly less in number than in the case of wild-type N3ECD. These results indicated that the process of degradation of mutant N3ECD on the cell surface is disturbed due to impairment of transendocytosis. Such disturbance on the surface of vascular smooth muscle cells may contribute to the pathogenesis of CADASIL.

Introduction

Cerebral autosomal dominant arteriopathy with subcortical infarcts and leukoencephalopathy (CADASIL) is characterized by migraine, cognitive impairment, depression, recurring subcortical infarcts, and dementia. Its pathological hallmark is systemic angiopathy affecting mainly small and medium-size arteries. These vascular lesions are characterized by degeneration of vascular smooth muscle cells (VSMCs), strongly stained with antibody to the extracellular domain of NOTCH3 (N3ECD), and exhibit the presence of granular osmiophilic material (GOM) (Joutel et al., 2000; Ruchoux et al., 1994). *NOTCH3* has been identified as a causative gene for CADASIL (Joutel et al., 1996), and the *NOTCH3* mutations in CADASIL patients are either missense mutations or small in-frame deletions coding the EGF-like repeats of NOTCH3. The Notch signaling pathway is an evolutionarily conserved intercellular signaling mechanism that controls vascular development and homeostasis (Lawson and Weinstein, 2002; Shawber and Kitajewski, 2004) as well as the development of most vertebrate organs (Artavanis-Tsakonas et al., 1999). *NOTCH3* is predominantly expressed in the VSMCs of late embryos and adults (Joutel et al., 2000), and defects in *NOTCH3* result in abnormalities of arterial structure and myogenic responses (Domenga et al., 2004).

Since the causative *NOTCH3* mutations for CADASIL result in an odd number of cysteine residues in the EGF-like repeats, the formation of abnormal disulfide bridges has been believed to affect ligand binding and signal transduction (Joutel et al., 1997). However, it remains unclear whether CADASIL mutations affect receptor trafficking and signaling. Previous studies suggested that most of the mutations located outside of the ligand-binding site did not impair the signal transduction activity of NOTCH3 (Low et al., 2006; Monet-Leprêtre et al., 2009). In addition, total loss of NOTCH3 did not cause CADASIL pathology in knock-out-mice (Kitamoto et al., 2005), suggesting that the mutant NOTCH3 protein plays a novel pathogenic role in gain of toxic function rather than compromise the canonical NOTCH3 function. The cytotoxic effect of mutant NOTCH3 due to the increase in endoplasmic reticulum (ER) stress has been hypothesized, based on experiments using cultured cells (Takahashi et al., 2010). However, previous studies were performed using overexpression of NOTCH3 in cultured cells. In general, misfolded mutant proteins overexpressed in cultured cells accumulate in ER and consequently induce ER stress (Mori, 2000). While the ER stress-induced cytotoxic effect of mutant

* Corresponding author at: Department of Neurology, Kyoto Prefectural University of Medicine, Kajiicho-465, Kamigyo-ku, Kyoto 602-8566, Japan. Fax: +81 75 211 8645.
E-mail address: mizuno@koto.kpu-m.ac.jp (T. Mizuno).

0014-4886/$ – see front matter © 2011 Elsevier Inc. All rights reserved.
doi:10.1016/j.expneurol.2011.10.020

NOTCH3 can explain the degeneration and loss of VSMCs in CADASIL, it is unclear whether this effect of mutant NOTCH3 induces the pathological findings of CADASIL, such as abnormal accumulation of N3ECD in vascular walls (Joutel et al., 2000, 2001).

The Notch receptor is believed to undergo a complex series of proteolytic processing events. The first cleavage of the receptor, the S1 cleavage, occurs in the Golgi apparatus by furin-like convertase (Logeat et al., 1998). The S2 cleavage occurs at the cell surface when the receptor interacts with ligand, Jagged, or DSL (Delta/Serrate/LAG-2), which are transmembrane proteins expressed on neighboring cells (Brou et al., 2000). The S3 cleavage is followed by constitutive γ-secretase-dependent intra-membrane proteolysis, and releases the Notch intracellular domain (NICD) into the cytoplasm. NICD then shuttles to the nucleus to associate with transcriptional cofactors of the CBF1-Su(H)-Lag1 (CSL) family and activate target genes (Bray, 2006). Recently, endocytosis of either the DSL ligands or the Notch receptor itself into the cytoplasm has been recognized to play an important role in regulating Notch signal (Bray, 2006; Fortini and Bilder, 2009; Pratt et al., 2011). In addition, recent genetic and cellular biological studies have shown that Notch is endocytosized into ligand-expressing neighboring cells in *Drosophila* (Klueg and Muskavitch, 1999), and that endocytosis of Notch extracellular domain (NECD) promotes Notch proteolysis and downstream signaling in mammals (Nichols et al., 2007). Therefore, endocytosis of NECD into ligand-expressing cells, called transendocytosis, is now believed to be more critical for Notch activation than proteolytic events (Nichols et al., 2007).

We hypothesized that mutant NOTCH3 protein, particularly N3ECD, may be refractory to degradation on the cell surface due to impaired transendocytosis into ligand-expressing cells with activation of Notch signaling. This hypothesis can easily explain abnormal accumulation of N3ECD in CADASIL vascular wall without accumulation of the intracellular domain of NOTCH3 (N3ICD) or full-length protein, since mutant NOTCH3 is similarly cleaved as well as wild-type NOTCH3 and signaling is activated normally. This hypothesis can also explain why mutant N3ECD associates with accumulation of GOM (Ishiko et al., 2006), close to the cell surface of VSMCs, and not within VSMCs.

To investigate the process of degradation and transendocytosis of N3ECD, we established a co-culture system in which cells expressing one copy of NOTCH3 using the Flp-In T-REx system were co-cultured with ligand Jagged1 (Jag1)-expressing cells. This system enables alleviation of the effects of overexpression NOTCH3, such as ER stress.

Materials and methods

Stable cell lines

HEK293 and Flp-In T-REx 293 cells were grown in Ham's F12 containing 10% fetal bovine serum and antibiotics. cDNAs encoding CADASIL mutation (C185R) and wild-type NOTCH3 carrying a hemagglutinin (HA) tag at the C terminus were donated. The *NheI–XhoI* fragments of these plasmids containing the Notch3-HA coding region were cloned into the pcDNA5/FRT/TO vector (Invitrogen, Carlsbad, CA, USA). These plasmids were co-transfected into Flp-In-T-REx 293 cells at the rate of 9:1 with Lipofectamine LTX (Invitrogen). Forty-eight hours later, cells were selected in Ham's F12 with 200 μg/ml hygromycin B, and screened for recombinant protein expression and FRT recombination. For production of a stable cell line expressing Jagged1 (Jag1)-HA protein, HEK293 cells were transfected with Jag1-HA pIRES plasmid (Koutelou et al., 2008) and pEGFP-N1 using Lipofectamine LTX. Stable cell lines were generated by recovering and expanding individual colonies after culturing the cells for 2 weeks in the presence of Neomycin. GFP-positive colonies were picked up, followed by confirmation of Jag1 expression by western blotting (Supplemental Fig. 1).

Western blotting

Cells were washed with PBS and extracted with PBS containing 0.5% Triton X-100 and protease inhibitor cocktail (Nacalai Tesque, Kyoto, Japan). Samples were separated by 7.5% SDS-polyacrylamide gel electrophoresis and transferred onto PVDF membranes (Millipore Corp., Billerica, MA, USA). After blocking, the membranes were incubated in primary antibodies (described below) overnight, washed, and then incubated in alkaline phosphate-conjugated goat anti-mouse IgG (Jackson ImmunoReseach Laboratories Inc., West Grove, PA) or goat anti-rabbit IgG (MP Biomedicals, Solon, OH) for 3 h. Immunosignals were detected with nitroblue tetrazolium chloride and 5-bromo-4-chloro3′-indolylphsphatase p-toluidine salt reagents. The band intensity was measured by Image J analysis (Abramoff et al., 2004).

Immunocytochemistry

Cells (1×10^5) were plated on round cover glasses (13 mm in diameter) with tetracycline (2 μg/ml). After being washed with PBS, they were then fixed with 4% paraformaldehyde for 30 min and permeabilized with 0.1% Triton X-100 in PBS for 5 min. After washing with PBS, cells were incubated with the primary antibodies (1:100) in a blocking solution (Nacalai Tesque) overnight. After three washes with PBS, the cells were incubated with fluorescein isthiocyanate (FITC)-conjugated anti-mouse IgG (1:500) or Alexa Fluor 546-conjugated anti-rabbit IgG (1:500) for 4 h at room temperature. After washing and staining with 4′,6-diamidino-2-phenilindole (DAPI) (Dojindo, Kumamoto, Japan), the cells on the cover glasses were mounted on glass slides in an aqueous mounting medium (GEL/MOUNT; Biomeda, Foster City, CA, USA) and imaged using a BZ-9000 fluorescence microscope (KEYENCE, Osaka, Japan) and with 8-bit resolution by taking single z-stack steps.

Antibodies

The following antibodies were used in immunocytochemistry and western blotting: mouse monoclonal anti-NOTCH3 antibody (Abnova, Taipei, Taiwan), rabbit polyclonal anti-NOTCH3 antibody (Abcam, Cambridge, USA), rabbit monoclonal anti-Jagged1 antibody (Cell Signaling Technology, Danvers, MA, USA), mouse monoclonal anti-HA antibody (Roche, Basel, Schweiz) and mouse monoclonal panactin antibody (Thermo Scientific, Waltham, MA, USA).

Ligand/receptor co-culture assay

Stable HEK293 cell lines expressing wild-type or mutant NOTCH3 (2×10^5) were plated overnight in 35 mm dishes until 50% confluent with tetracycline 2 μg/ml. The Jagged1-expressing or GFP cells (2×10^5) were mixed with either dish. After 24 h, total RNAs were prepared from these cultures for examination of Notch signaling activity. Preparation of total RNA was performed with the RNeasy Micro Kit (QIAGEN, Hilden, Germany) and synthesis of cDNA was performed with the ThermoScript RT-PCR System (Invitrogen). The level of expression of HES-1 gene was measured by quantitative PCR as an index of Notch3 activity.

The PCR primer sequences for HES1 and G3PDH were as follows: HES1, forward primer, 5′-TGAAGGATTCCAAAAATAAAATTCTCTGGG-′3; reverse primer, 5′-CGCCTCTTCTCCTGATAGGCTTTGATGAC-′3, G3PDH, forward primer, 5′-ATGATTCTACCCACGGCAAG-′3; reverse primer 5′-CTGGAAGATGGTGATGGGTT-′3. Quantitative PCR was carried out using the Thermal Cycler Dice Real Time System (Thermal Cycler Dice, Takara Bio Inc., Otsu, Japan). The PCR amplification was performed for 40 cycles of 95 °C for 5 s and 60 °C for 30 s using SYBR premix EX TaqII (Takara Bio Inc.).

Please cite this article as: Watanabe-Hosomi, A., et al., Transendocytosis is impaired in CADASIL-mutant NOTCH3, Exp. Neurol. (2011), doi:10.1016/j.expneurol.2011.10.020

Biotinylation experiment

Cultures of the stable HEK293 cell lines in 35 mm dishes were incubated with 0.25 mg/ml Sulfo-NHS-SS-biotin (Pierce, Rockford, USA) for 1 h at 4 °C. Cells were washed three times with TBS and subsequently lysed with 1% TritonX-100 and protease inhibitor cocktail (Nacalai) in TBS. The lysate was incubated with 100 μg of streptavidin-coated magnetic beads (Promega Corporation, Madison, WI, USA) overnight at 4 °C. The beads were magnetically captured and washed with 500 μl ice-cold PBS twice. Biotinylated proteins were recovered in 50 μl of SDS/PAGE loading buffer and further processed by western blotting. The biotinylated proteins captured by streptavidin-coated beads were confirmed by western blotting (Supplemental Fig. 2).

Statistical analysis

Values are presented as means ± SD. Statistical analysis was performed using Bonferroni and one-way ANOVA with Dunnett's multiple comparison post hoc test (Dr. SPSS II, SPSS Inc., Chicago, IL, USA). Values of $P<0.05$ were considered significant.

Results

NOTCH3 expression in HEK293 cells

We first assessed NOTCH3 expression with transient transfection in cultured cells. However, transiently transfected NOTCH3 proteins exhibited a tendency to form aggregates intracellularly with either wild-type or C185R mutant, and consequently caused cell death. To alleviate the effects of NOTCH3 overexpression, we established stable HEK293 cell lines carrying one copy of wild-type (W) or C185R mutant NOTCH3 using the Flp-In T-REx system regulated by tetracycline. Three colonies for each construct were selected for subsequent experimentation. The 280 and 95 kDa bands were detected with an antibody to N3ICD in the stable cell lines expressing NOTCH3 induced by tetracycline (Figs. 1A and B, left). The anti-N3ECD antibody detected two immunoreactive bands at 280 and 210 kDa (Fig. 1B, right). The results of western blotting indicated that the 280, 210, and 95 kDa bands corresponded to the full length of NOTCH3, N3ECD, and N3ICD, respectively. We examined the expression and localization of NOTCH3 in our established cells immunocytochemically (Fig. 1C). Both wild-type and C185R mutant NOTCH3 were similarly detected on the cell surface. No difference was detected in proliferation between wild-type and mutant cell lines.

Degradation of wild-type and mutant NOTCH3

Our stable NOTCH3 cell lines expressing one copy of both wild-type and C185R mutation did not have the propensity to form intracellular aggregates, nor did they tend to suppress proliferation. We therefore evaluated degradation of NOTCH3 protein in wild-type and C185R mutation cells using the tetracycline-regulating system.

Each stable cell line was incubated with tetracycline (Tet-on) for two days, and then cells were incubated for one to five days in the absence of tetracycline (Tet-off) (Fig. 2A). Each cell lysate was subjected to western blotting with anti-N3ECD (upper), anti-N3ICD (middle), and anti-actin (lower) antibodies, and relative band intensities were calculated with the Tet-off 0 day band intensity considered 100%. Two days after Tet-off, full length (FL), N3ECD, and N3ICD levels were decreased to 20–30%, and these turnover rates did not differ between the wild-type and C185R mutant (Figs. 2A, B).

Degradation of wild-type or mutant NOTCH3 with ligand-expressing cells

While NOTCH3 is degraded by the multi-vesicular body pathway in the NOTCH3-expressing cell itself (Bray, 2006), NOTCH3 is speculated to be transendocytosized and degraded by the ligand-expressing cells. To evaluate the effects of ligand on the degradation of NOTCH3, we designed a co-culture assay of NOTCH3-expressing cells with Jagged1-expressing cells. After the HEK293 cells expressing wild-type or C185R mutant NOTCH3 were incubated with tetracycline for one day,

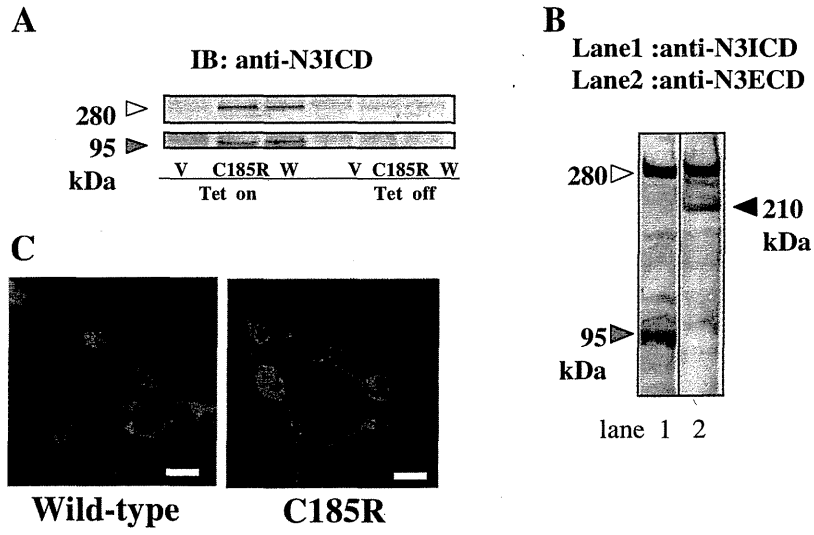

Fig. 1. Expression of wild-type and C185R mutant NOTCH3 in stable HEK 293 cells induced by the Flp-In T-REx system. A. Stable cell lines transfected with vector (V), wild-type (W), or C185R mutant (C185R) NOTCH3 were generated using Flp-In integration. Expression of either wild-type or C185R NOTCH3 protein was confirmed by immunoblotting with the antibody to intracellular domain of NOTCH3 (anti-N3ICD). Cells were incubated with tetracycline (Tet on) or without tetracycline (Tet off). The full length (FL) and NOTCH3 intracellular domain (N3ICD) were detected when cells expressing wild-type or C185R mutant NOTCH3 were cultured with tetracycline. No band was detected when cells were cultured without tetracycline. B. Cell lysate from stable cells of wild-type NOTCH3 were subjected to immunoblotting analysis using anti-N3ICD:Lane 1 or anti-NOTCH3 extracellular domain (N3ECD):Lane 2. The immunoreactive bands at 280 and 95 kDa were detected with anti-N3ICD antibody indicating FL and N3ICD, respectively, while the bands at 280 and 210 kDa with anti-N3ECD antibody indicating FL and N3ECD, respectively. C. Immunocytochemical analysis of single-copy transformants of either wild-type or C185R mutant NOTCH3 using anti-N3ECD antibody revealed the distribution of NOTCH3 at the cell surface. Scale bar: 10 μm.

Please cite this article as: Watanabe-Hosomi, A., et al., Transendocytosis is impaired in CADASIL-mutant NOTCH3, Exp. Neurol. (2011), doi:10.1016/j.expneurol.2011.10.020

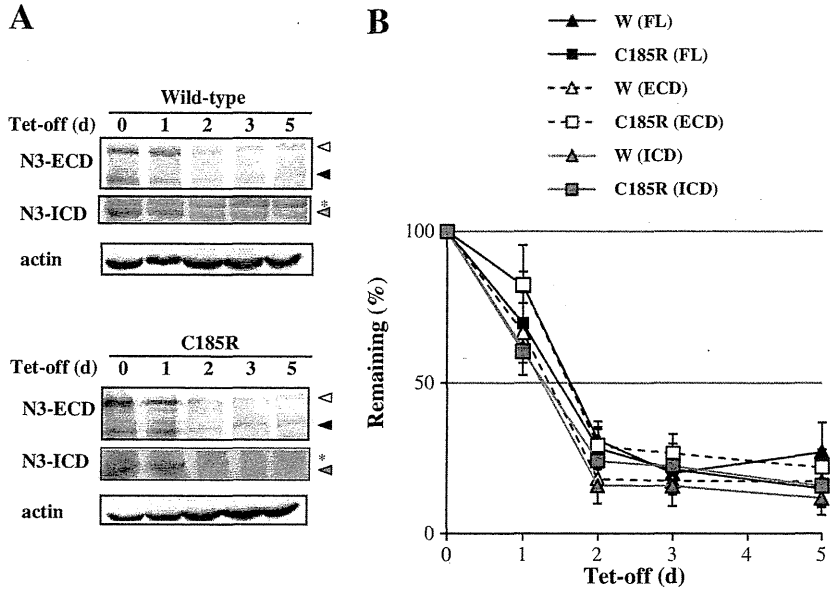

Fig. 2. Degradation of wild-type and C185R mutant NOTCH3. A. Stable cell lines were treated with tetracycline (Tet-on) for two days, and cells were then incubated for one to five days in the absence of tetracycline (Tet-off). Each cell lysate was subjected to western blotting with anti-N3ECD (upper), anti-N3ICD (middle), and anti-actin (lower) antibodies. FL, N3ECD, and N3ICD of wild-type or mutant NOTCH3 were similarly degraded within 5 days. Open arrowheads, closed arrowheads (black), and closed arrowheads (gray) indicated FL, N3ECD, and N3ICD of NOTCH3, respectively. Asterisks indicate non-specific bands. B. The relative band intensity of each cell lysate on western blotting in panel A was calculated with Tet-off 0 day band intensity considered 100%. The degradation of FL, N3ECD, and N3ICD did not differ significantly between wild-type and C185R NOTCH3. Values represent means ± SD of data from three independent experiments. Open triangles: W-ECD, closed triangles (black): W-FL, closed triangles (gray): W-ICD, open squares: C185R-ECD, closed squares (black): C185R-FL, closed squares (gray): C185R-ICD.

the Jagged1-expressing cells (293-Jag1) or the GFP-expressing cells (293-GFP) as a control were co-cultured. The following day, the medium was changed to one without tetracycline and then the cells were incubated for one to five days (Fig. 3A). The efficiency for co-culture system on Notch signal was confirmed by HES1 signaling activity with quantitative RT-PCR (Fig. 3B). In addition, we ascertained that HES1 signal was derived from NOTCH3 cells, because HES1 signals from 293-Jag1 and 293-GFP were similar (Supplemental Fig. 3). To evaluate degradation of NOTCH3 under co-culture conditions, western blotting of total cell lysate in each sample was performed. The relative band intensity of each cell lysate on western blotting was calculated with Tet-off 0 day band intensity considered 100%. One day after Tet-off, turnover of wild-type NOTCH3 FL was significantly reduced by co-culture with 293-Jag1 cells. On the other hand, C185R mutant did not significantly differ in FL turnover between 293-Jag1 and 293 GFP co-cultured cells (Figs. 3C, D). Turnover of N3ECD and N3ICD did not differ significantly between wild-type and C185R mutant.

Since the large proportion of NOTCH3 proteins was degraded during initial 2 days, we examined the turnover of NOTCH3 protein with greater sampling frequency within the first 2 days. The degradation of N3FL, N3ECD and N3ICD did not significantly differ in the first 2 days (Supplemental Fig. 4).

NOTCH3 kinetics on the cell surface

In the examination using total lysate, wild-type and C185R mutant NOTCH3 displayed modest change in turnover of FL form under 293-Jag1 co-culture conditions. A large amount of NOTCH3 protein is assumed to exist inside cell organelles such as endoplasmic reticulum (ER) or lysosomes (Karlström et al., 2002; Takahashi et al., 2010). We next evaluated the degradation of NOTCH3 on the cell surface. Similarly, NOTCH3 cells were co-cultured with 293-Jag1 or GFP cells in medium containing tetracycline. We then performed cycloheximide (CHX)-chase analysis to stop protein synthesis, since cell surface NOTCH3 is a short-lived protein. Tetracycline was removed from the medium and CHX (50 μg/ml) was added to suppress the translation of NOTCH3. Cell surface proteins were biotinylated by Sulfo-NHS-SS-Biotin, followed by streptavidin pull-down assays and western blotting, after 0, 3, and 6 h of CHX-chase (Fig. 4A). The vast majority of the protein captured by the streptavidin beads was N3ECD, and neither FL nor NICD, indicating

Fig. 3. Degradation of wild-type or C185R mutant NOTCH3 with ligand-expressing cells. A. HEK293 cells expressing wild-type or C185R mutant NOTCH3 were co-cultured with HEK293 expressing Jag1 (293-Jag1) or HEK293 expressing GFP (293-GFP) cells for one day. For evaluation of the turnover of FL, N3ECD, and N3ICD from wild-type (W) or C185R mutant NOTCH3, co-cultured cells were chased in medium without tetracycline for 0–5 days. The total lysate of each cell was analyzed by western blotting with anti-N3ECD anti-N3ICD, and anti-actin antibodies. B. Expression of HES1 was assessed by real-time PCR. HES1 was significantly more activated in either wild-type or C185R mutant NOTCH3 co-culture with 293-Jag1 than co-culture with 293-GFP. Values represent the means ± SD of data from three independent experiments. ** indicates $P<0.01$ compared to co-culture with 293-GFP. C. Western blotting of NOTCH3 using total cell lysate. FL of wild-type NOTCH3 with 293-Jag1 after Tet-off decreased more rapidly than without 293-Jag1. FL of mutant NOTCH3 exhibited no significant difference with and without 293-Jag1. Both N3ECD and N3ICD were degraded similarly in HEK293 expressing wild-type or mutant NOTCH3 with or without 293-Jag1. Upper left: co-culture of W-NOTCH3 with 293-GFP, upper right: W-NOTCH3 with 293-Jag1, lower left: C185R NOTCH3 with 293-GFP, and lower right: C185R NOTCH3 with 293-Jag1. Open arrowheads, closed arrowheads (black), and closed arrowheads (gray) indicate FL, N3ECD and N3ICD, respectively. Asterisks indicate non-specific bands. D. FL of W-NOTCH3 with 293-Jag1 was degraded significantly more rapidly than C185R with 293-Jag1 or W-NOTCH3 with 293-GFP at Tet-off 1 day. The degradation of N3ECD and N3ICD did not differ significantly between wild-type and C185R NOTCH3. The relative band intensity of each cell lysate on western blotting was calculated with Tet-off 0 day band intensity considered 100%. Values represent means ± SD of data from three independent experiments. * indicates $P<0.05$ when the relative band intensity of the FL of W-NOTCH3 with 293-Jag1 was compared with the FL of W-NOTCH3 with 293-GFP. Open triangles: co-culture of W-NOTCH3 with 293-GFP, closed triangles (black): W-NOTCH3 with 293-Jag1, open squares: C185R with 293-GFP, closed squares (black): C185R with 293-Jag1.

Please cite this article as: Watanabe-Hosomi, A., et al., Transendocytosis is impaired in CADASIL-mutant NOTCH3, Exp. Neurol. (2011), doi:10.1016/j.expneurol.2011.10.020

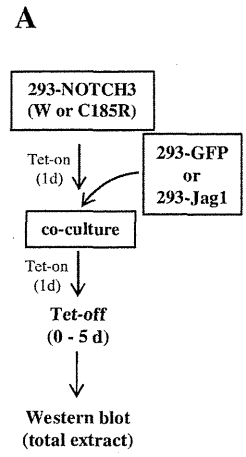

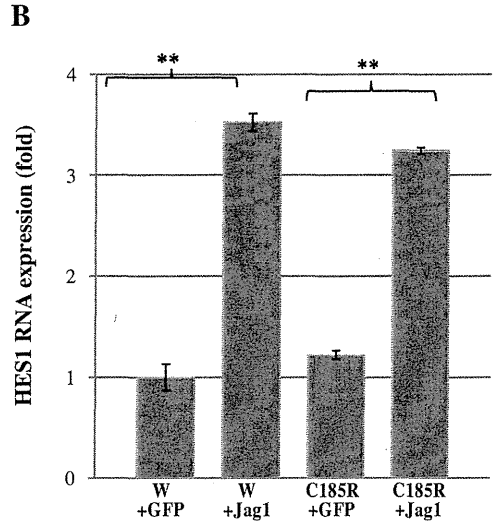

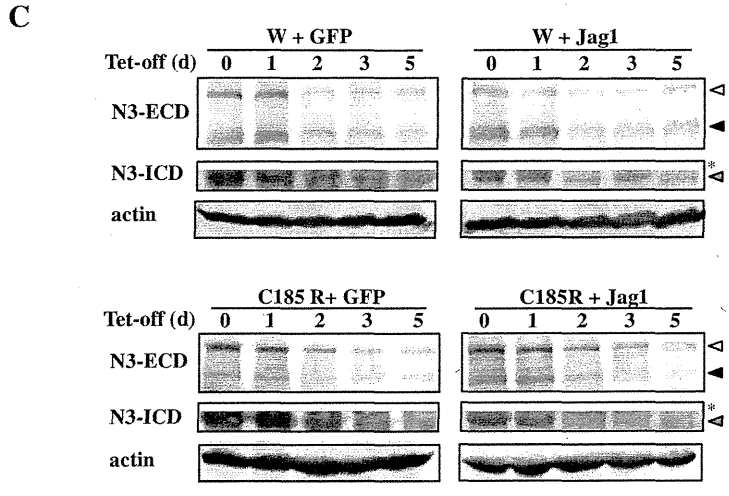

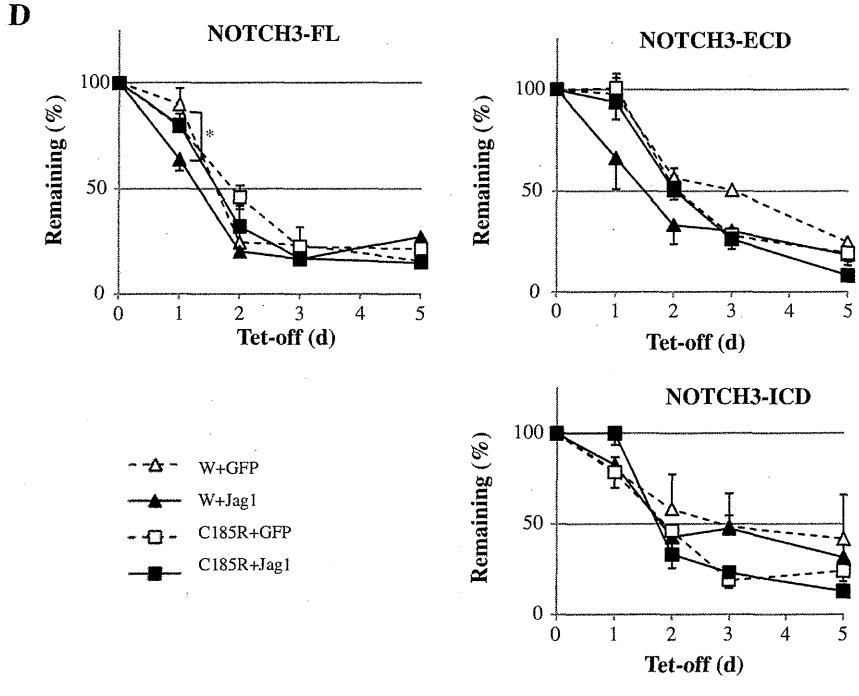

Please cite this article as: Watanabe-Hosomi, A., et al., Transendocytosis is impaired in CADASIL-mutant NOTCH3, Exp. Neurol. (2011), doi:10.1016/j.expneurol.2011.10.020

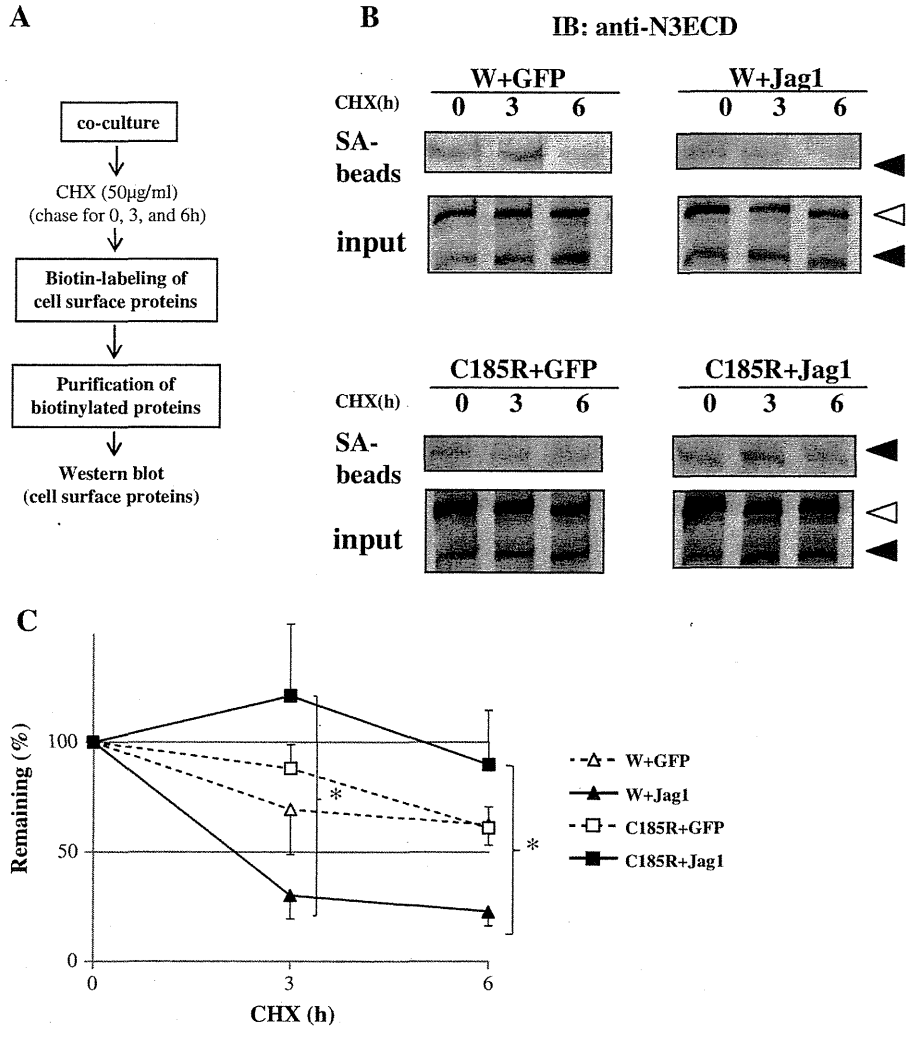

Fig. 4. NOTCH3 kinetics on the cell surface A. Wild-type or C185R NOTCH3 cells were plated with tetracycline and co-cultured with ligand-expressing cells as in Fig. 3. After tetracycline was removed from the medium, cycloheximide (CHX) (50 μg/ml) was added to stop NOTCH3 synthesis. Cell surface proteins were labeled with biotin and captured in streptavidin beads. NOTCH3 among biotinylated surface proteins and total lysates was analyzed by western blotting at 0, 3, and 6 h after discontinuation of synthesis. B. Western blotting of cell surface proteins. Biotinylated wild-type N3ECD with 293-Jag1 reduced more rapidly than C185R with 293-Jag1. Open arrowheads and closed arrowheads indicate FL, and N3ECD, respectively. Upper left: co-culture of W-NOTCH3 with 293-GFP, upper right: W-NOTCH3 with 293-Jag1, lower left: C185R NOTCH3 with 293-GFP, and lower right: C185R NOTCH3 with 293-Jag1. SA-beads indicate the biotinylated proteins captured by streptavidin beads. Input indicates 5% of the protein extract from the total lysates that were removed before pull down with magnetic beads coupled to streptavidin. C. Biotinylated wild-type N3ECD with 293-Jag1 was degradated significantly more rapidly than biotinylated C185R N3ECD with 293-Jag1 or W-NOTCH3 with 293-GFP at 3 and 6 h after CHX was added. The relative band intensity of each cell lysate on western blotting was calculated with Tet-off 0 day band intensity considered 100%. Values represent means ± SD of data from three independent experiments. * indicates $P<0.05$ when the relative band intensity of the W-NOTCH3 with 293-Jag1 was compared with C185R NOTCH3 with 293-Jag1. Open triangles: co-culture of W-NOTCH3 with 293-GFP, closed triangles (black): W-NOTCH3 with 293-Jag1, open squares: C185R with 293-GFP, closed squares (black): C185R with 293-Jag1.

that only the mature form on NOTCH3 was located on the cell surface. Input proteins indicate intracellular N3ECD and N3FL before pull down with magnetic beads coupled to streptavidin. The degradation of intracellular N3ECD and N3FL was modest within 6 h (Fig. 4B). In the absence of 293-Jag1, there was no difference in half-life of cell surface N3ECD between wild-type and C185R mutation (Figs. 4B, C). On the other hand, N3ECD on the cell surface was significantly decreased to 20–30% 6 h after CHX when wild-type NOTCH3 cells were co-cultured with 293-Jag1 (Fig. 4B, upper right panel, Fig. 4C). However, induction of N3ECD degradation by 293-Jag1 was less observed in C185R mutation

Fig. 5. NOTCH3 exists in ligand-expressing cells. A. NOTCH3 cells were treated with 2 μg/ml tetracycline for 24 h and then 293-Jag1 or 293-GFP was added and incubated for two days with tetracycline. The cells were fixed and double-stained with antibody. The left panels represent wild-type and C185R NOTCH3 stained with anti-N3ECD antibody (red). The middle panels represent Jag1 or GFP-expressing cells (green). The right panels show an overlay (merge). Vesicles stained with anti-N3ECD antibody exist within wild-type as well as C185R NOTCH3 cells. Vesicles stained with anti-N3ECD antibody also exist within 293-Jag1 (open arrow). Scale bar: 10 μm. B. The proportion of ligand-expressing cells with N3ECD-positive vesicles on co-culture. 293-Jag1 or GFP cells with N3ECD-positive vesicles were quantified manually by counting cell numbers and scored as the percentage of the total number of 293-Jag1 or GFP cells. The percentage of 293-Jag1 cells with N3ECD-positive vesicles on co-culture with W-NOTCH3 was about 70%, and significantly higher than with C185R NOTCH3. The percentage of cells with N3ECD-positive vesicles was also significantly higher in 293-Jag1 than in 293-GFP on co-culture with W-NOTCH3. * indicates $P<0.05$ relative to co-culture of W-NOTCH3 cells with 293-Jag1 cells. C. The percentage of N3ECD-positive vesicles in NOTCH3 cells was similar with either co-culture combination. Values represent means ± SD of data from three independent experiments.

Please cite this article as: Watanabe-Hosomi, A., et al., Transendocytosis is impaired in CADASIL-mutant NOTCH3, Exp. Neurol. (2011), doi:10.1016/j.expneurol.2011.10.020

(Fig. 4B, lower right panel, Fig. 4C). The C185R mutant N3ECD on the cell surface (closed squares) was degraded significantly more slowly than the wild NOTCH3 (closed triangle) when NOTCH3 cells were co-cultured with Jag1 expressing cells. This result indicates that degradation of mutant NOTCH3 on the cell surface was retarded.

NOTCH3 exists in ligand-expressing cells

The Notch pathway is activated by the endocytic trafficking of ligands and receptors, particularly when the receptors are internalized into signal-sending cells in transendocytosis (Bray, 2006; Nichols

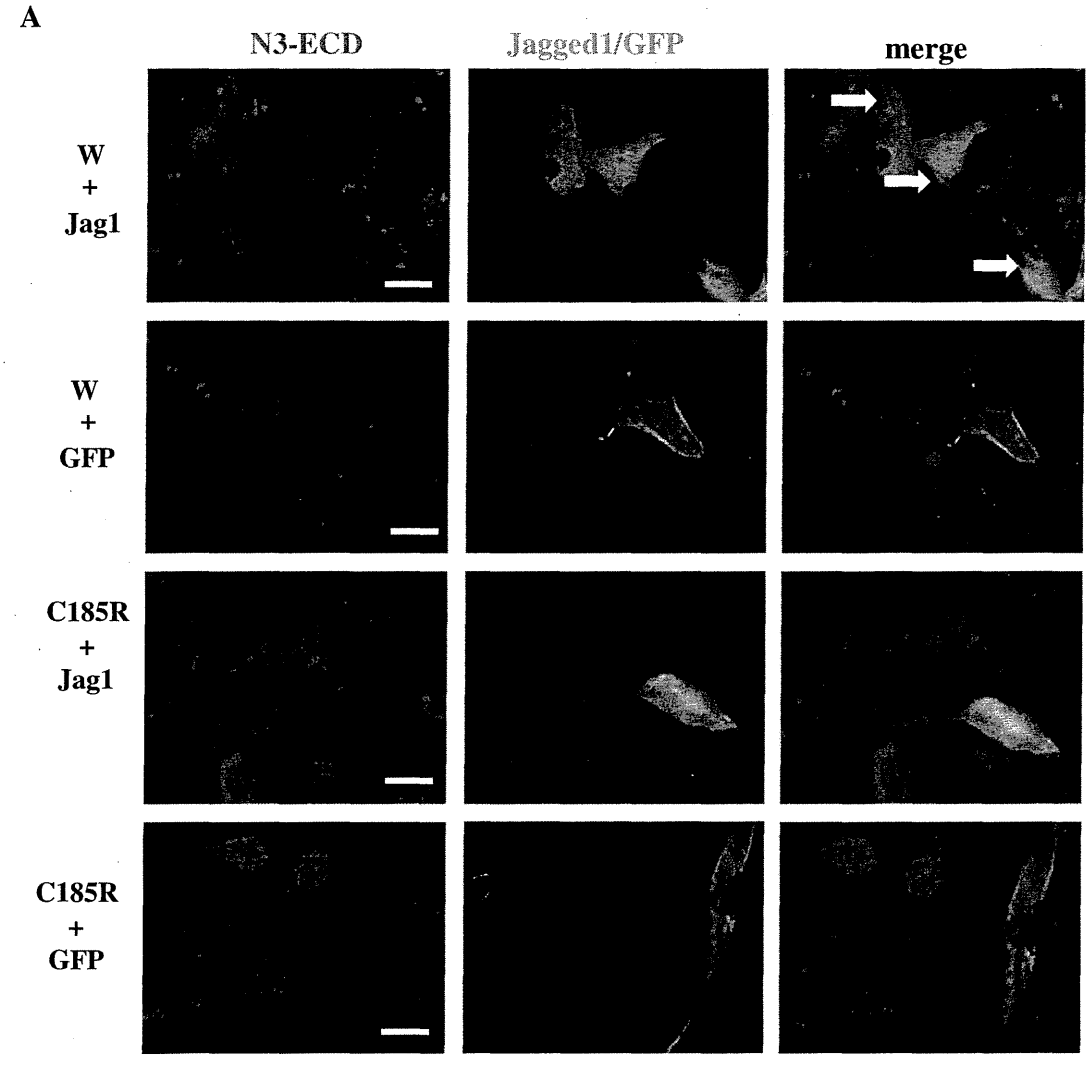

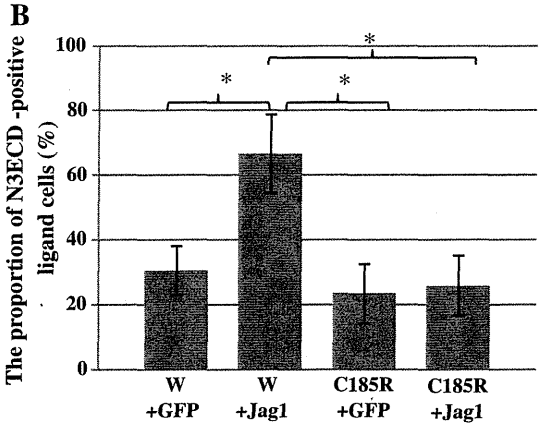

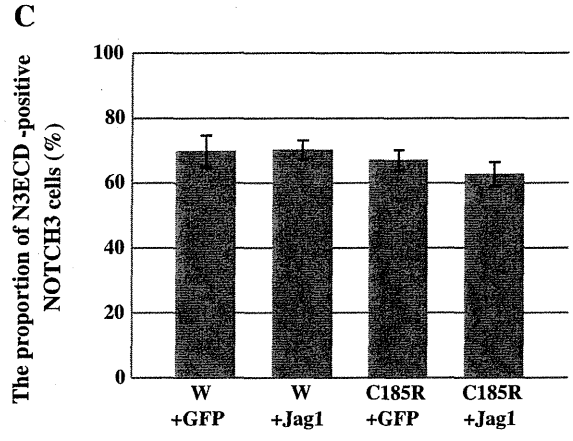

Please cite this article as: Watanabe-Hosomi, A., et al., Transendocytosis is impaired in CADASIL-mutant NOTCH3, Exp. Neurol. (2011), doi:10.1016/j.expneurol.2011.10.020

et al., 2007; Pratt et al., 2011). We speculated that CADASIL mutation may delay N3ECD degradation via its transendocytosis. We then immunocytochemically investigated the transendocytosis of N3ECD into 293-Jag1 cells. On this analysis, punctate signals were detected in 293-Jag1 cells with anti-N3ECD antibody when wild-type NOTCH3 cells were co-cultured (Fig. 5A, upper panel; arrows). This observation suggests incorporation of wild-type N3ECD into 293-Jag1 cells via its transendocytosis. Although some vesicles stained by anti-N3ECD antibody were detected within the 293-Jag1 cells when mutant NOTCH3 cells were co-cultured, transendocytic vesicles of mutant N3ECD were fewer in number than those of wild-type N3ECD (Fig. 5A, third panels). Transendocytosis was quantified by counting N3ECD-positive vesicles in the 293-Jag1 or GFP cells manually (Fig. 5B). The N3ECD-positive vesicles were detected in about 70% of 293-Jag1 cells on co-culture of wild-type NOTCH3 with 293-Jag1 cells, suggesting that NOTCH3 transendocytosis is possible, as previously reported for Notch1 (Nichols et al., 2007). On the other hand, in other combinations of co-culture, the N3ECD-positive vesicles were detected in about 30% of 293-Jag1 or GFP cells. Efficient transendocytosis of wild-type N3ECD may contribute to the rapid degradation of N3ECD on the cell surface, and disturbance of the transendocytosis of the mutant N3ECD may yield accumulation of mutant N3ECD on the cell surface. There were no differences in the proportion of N3ECD-positive vesicles within the NOTCH3 cells with either combination (Fig. 5C).

Discussion

We detected vesicles of N3ECD within most Jag1-expressing cells and increase in HES1 expression in NOTCH3 cells on co-culture of Jag1-expressing cells. Our findings are in agreement with a recent proposed model by Nichols et al. (2007) for the transduction of biological signals in the Delta/Notch pathway (Nichols et al., 2007). They proposed that Notch activity is promoted by transendocytosis that mechanically stresses the Notch heterodimer, resulting in proteolytic activation of Notch. They observed that the Notch1 extracellular domain (N1ECD) including Notch1 receptors was transferred to and taken up by ligand-expressing cells, and that these events correlate with activated NICD in the nucleus of contacted Notch cells. In addition, both dissociation of receptor and internalization of NECD into ligand-expressing cells require Notch maturation by furin processing, but occur independent of ADAM proteolysis. We confirmed transendocytosis of wild-type N3ECD as well as N1ECD in our co-culture system.

Interestingly, N3ECD vesicles in the ligand-expressing cells accumulated less on co-culture with mutant NOTCH3 cells than with wild-type NOTCH3 cells. These present findings suggested that transendocytosis of mutant NOTCH3 by ligand-expressing cells might be disturbed. Our findings for NOTCH3 kinetics on the cell surface showed that the C185R mutant N3ECD was degraded significantly more slowly than the wild-type N3ECD. These findings suggest that the complex of mutant N3ECD and ligand can be left on the cell membrane due to the impairment of transendocytosis, while wild-type N3ECD is rapidly taken up and endocytosized by ligand-expressing cells. The previous study revealed that mutant N3ECD could be accumulated on the cell surface of HEK293 cells transiently expressing mutant NOTCH3 with direct administration of Notch ligand (Haritunians et al., 2002). In the case of Notch1, the complex of N1ECD and ligands was detected on the cell surface of both Notch and ligand-expressing cells when Notch1 cells were co-cultured with Delta like 1 or jagged (Nichols et al., 2007). Opherk et al. (2009) showed that CADASIL-associated mutations significantly enhance NOTCH3 multimerization mediated by disulfide bonds compared with wild NOTCH3 in vitro (Opherk et al., 2009). In addition, accumulation of N3ECD was detected within the GOM deposits (Ishiko et al., 2006), suggesting that mutant NOTCH3 may associate with accumulations of GOM. GOM deposits are located extracellularly, close to the cell surface of VSMCs, and not within VSMCs. In our study, we demonstrated the possibility that mutant N3ECD remains on the cell surface, compatible with the pathological findings of CADASIL. Our study can also explain the strong N3ECD staining around small arteries in CADASIL brain (Joutel et al., 2000).

Our study revealed that some N3ECD vesicles in the ligand-expressing cells accumulated when mutant NOTCH3 cells were co-cultured either with or without ligand-expressing cells. This result raises a question that mutant NOTCH3 may suppress endocytosis and inhibit Notch signal. However, this is unlikely, since Notch signal was activated similarly by both wild-type and mutant NOTCH3, based on results of HES1 induction. Previous studies generating NOTCH3 mutant protein on co-culture with Notch ligand also showed that the NOTCH3 mutant protein did not affect cleavage, binding capacity to the Notch ligand, or CBF1 activation (Haritunians et al., 2005; Low et al., 2006).

Takahashi et al. (2010) observed that mutant NOTCH3 is more prone to form aggregates than wild-type NOTCH3 and that the mutant aggregates are resistant to degradation, leading to their accumulation in the ER (Takahashi et al., 2010). They speculated that aberrant disulfide linking in mutant NOTCH3 increases the formation of aggregates and impairs the interaction with ER chaperones and proteases for efficient degradation, ultimately impairing cell proliferation. We used the Flp-In T-REx system in this study because we found toxic effects of NOTCH3 overexpression on cell growth in our preliminary experiments (data not shown). The Flp-In T-REx system has the advantage of expressing one copy of NOTCH3 in HEK293, since one copy of mutant NOTCH3 is more representative of the pathology of CADASIL more than overexpression of mutant NOTCH3. In addition, Flp-In T-REx 293 cells in this system are derived from the HEK 293. The fundamental nature of the Flp-In T-REx 293 cells is similar to HEK 293, which are the most popular cell lines expressing mutant NOTCH3 in the other previous studies. In our experiment, some vesicles stained with anti-N3ECD antibody were observed within either wild-type or mutant NOTCH3 cells, but no toxicity was detected for surviving and proliferating cells and there was also no difference in the degradation of NOTCH3. Our data supported that the vesicles stained with NOTCH3 antibodies might be a physiological condition such as endosome or lysosome (Kanwar and Fortini, 2004).

Several issues remain in the investigation of the degradation of mutant NOTCH3. In our biotinylation experiments on cell surface proteins, we could not determine whether N3ECD resides in NOTCH3 cells or ligand-expressing cells. To determine with precision the mechanism of degradation of N3ECD on the cell surface, further studies will be necessary. Whether our results showing the impairment of transendocytosis could be observed in smooth muscle cells is an important next issue. To elucidate the pathomechanism of CADASIL, other NOTCH3 mutations, particularly those occurring within the ligand binding site, should be verified. Nevertheless, our findings raise the possibility that degradation of mutant NOTCH3 on the cell surface might play a key role in the pathogenesis of CADASIL, and that clearance of mutant NOTCH3 will become a target of effective treatment or alleviation of CADASIL.

Acknowledgments

We thank Dr. Kalaria for the gift of cDNAs encoding the CADASIL mutation (C185R) and wild-type NOTCH3, and E. Koutelou for the gift of plasmid carrying Jagged1 through Addgene. This work was supported by grants from the Ministry of Education, Culture Sports, Science and Technology of Japan (22591595) and the Ministry of Health, Labor and Welfare of Japan (22141101).

Appendix A. Supplementary data

Supplementary data to this article can be found online at doi:10.1016/j.expneurol.2011.10.020.

References

Abramoff, M.D., Magelhaes, P.J., Ram, S.J., 2004. Image processing with ImageJ. Biophotonics Int. 11 (7), 36–42.

Artavanis-Tsakonas, S., Rand, M.D., Lake, R.J., 1999. Notch signaling: cell fate control and signal integration in development. Science 284, 770–776.

Bray, S.J., 2006. Notch signalling: a simple pathway becomes complex. Nat. Rev. Mol. Cell Biol. 7, 678–689.

Brou, C., Logeat, F., Gupta, N., Bessia, C., LeBail, O., Doedens, J.R., Cumano, A., Roux, P., Black, R.A., Israël, A., 2000. A novel proteolytic cleavage involved in Notch signaling: the role of the disintegrin-metalloprotease TACE. Mol. Cell. 5, 207–216.

Domenga, V., Fardoux, P., Lacombe, P., Monet, M., Maciazek, J., Krebs, L.T., Klonjkowski, B., Berrou, E., Mericskay, M., Li, Z., Tournier-Lasserve, E., Gridley, T., Joutel, A., 2004. Notch3 is required for arterial identity and maturation of vascular smooth muscle cells. Genes Dev. 18, 2730–2735.

Fortini, M.E., Bilder, D., 2009. Endocytic regulation of Notch signaling. Curr. Opin. Genet. Dev. 19, 323–328.

Haritunians, T., Boulter, J., Hicks, C., Buhrman, J., DiSibio, G., Shawber, C., Weinmaster, G., Nofziger, D., Schanen, C., 2002. CADASIL Notch3 mutant proteins localize to the cell surface and bind ligand. Circ. Res. 90, 506–508.

Haritunians, T., Chow, T., De Lange, R.P., Nichols, J.T., Ghavimi, D., Dorrani, N., St Clair, D.M., Weinmaster, G., Schanen, C., 2005. Functional analysis of a recurrent missense mutation in Notch3 in CADASIL. J. Neurol. Neurosurg. Psychiatry 76, 1242–1248.

Ishiko, A., Shimizu, A., Nagata, E., Takahashi, K., Tabira, T., Suzuki, N., 2006. Notch3 ectodomain is a major component of granular osmiophilic material (GOM) in CADASIL. Acta Neuropathol. 112, 333–339.

Joutel, A., Corpechot, C., Ducros, A., Vahedi, K., Chabriat, H., Mouton, P., Alamowitch, S., Domenga, V., Cécillion, M., Marechal, E., Maciazek, J., Vayssiere, C., Cruaud, C., Cabanis, E.A., Ruchoux, M.M., Weissenbach, J., Bach, J.F., Bousser, M.G., Tournier-Lasserve, E., 1996. Notch3 mutations in CADASIL, a hereditary adult-onset condition causing stroke and dementia. Nature 383, 707–710.

Joutel, A., Vahedi, K., Corpechot, C., Troesch, A., Chabriat, H., Vayssière, C., Cruaud, C., Maciazek, J., Weissenbach, J., Bousser, M.G., Bach, J.F., Tournier-Lasserve, E., 1997. Strong clustering and stereotyped nature of Notch3 mutations in CADASIL patients. Lancet 350, 1511–1515.

Joutel, A., Andreux, F., Gaulis, S., Domenga, V., Cecillon, M., Battail, N., Piga, N., Chapon, F., Godfrain, C., Tournier-Lasserve, E., 2000. The ectodomain of the Notch3 receptor accumulates within the cerebrovasculature of CADASIL patients. J. Clin. Invest. 5, 597–605.

Joutel, A., Favrole, P., Labauge, P., Chabriat, H., Lescoat, C., Andreux, F., Domenga, V., Cécillon, M., Vahedi, K., Ducros, A., Cave-Riant, F., Bousser, M.G., Tournier-Lasserve, E., 2001. Skin biopsy immunostaining with a Notch3 monoclonal antibody for CADASIL diagnosis. Lancet 358, 2049–2051.

Kanwar, R., Fortini, M.E., 2004. Notch signaling: a different sort makes the cut. Curr. Biol. 1043–1045.

Karlström, H., Beatus, P., Dannaeus, K., Chapman, G., Lendahl, U., Lundkvist, J., 2002. A CADASIL-mutated Notch 3 receptor exhibits impaired intracellular trafficking and maturation but normal ligand-induced signaling. Proc. Natl. Acad. Sci. U. S. A. 99, 17119–17124.

Kitamoto, T., Takahashi, K., Takimoto, H., Tomizuka, K., Hayasaka, M., Tabira, T., Hanaoka, K., 2005. Functional redundancy of the Notch gene family during mouse embryogenesis: analysis of Notch gene expression in Notch3-deficient mice. Biochem. Biophys. Res. Commun. 331, 154–162.

Klueg, K.M., Muskavitch, M.A., 1999. Ligand-receptor interactions and trans-endocytosis of Delta, Serrate and Notch: members of the Notch signalling pathway in *Drosophila*. J. Cell Sci. 112, 3289–3297.

Koutelou, E., Sato, S., Tomomori-Sato, C., Florens, L., Swanson, S.K., Washburn, M.P., Kokkinaki, M., Conaway, R.C., Conaway, J.W., Moschonas, N.K., 2008. Neuralized-like 1 (Neurl1) targeted to the plasma membrane by N-myristoylation regulates the Notch ligand Jagged1. J. Biol. Chem. 15, 3846–3853.

Lawson, N.D., Weinstein, B.M., 2002. In vivo imaging of embryonic vascular development using transgenic zebrafish. Dev. Biol. 248, 307–318.

Logeat, F., Bessia, C., Brou, C., LeBail, O., Jarriault, S., Seidah, N.G., Israël, A., 1998. The Notch1 receptor is cleaved constitutively by a furin-like convertase. Proc. Natl. Acad. Sci. U. S. A. 95, 8108–8112.

Low, W.C., Santa, Y., Takahashi, K., Tabira, T., Kalaria, R.N., 2006. CADASIL-causing mutations do not alter Notch3 receptor processing and activation. Neuroreport 17, 945–949.

Monet-Leprêtre, M., Bardot, B., Lemaire, B., Domenga, V., Godin, O., Dichgans, M., Tournier-Lasserve, E., Cohen-Tannoudji, M., Chabriat, H., Joutel, A., 2009. Distinct phenotypic and functional features of CADASIL mutations in the Notch3 ligand binding domain. Brain 132, 1601–1612.

Mori, K., 2000. Tripartite management of unfolded proteins in the endoplasmic reticulum. Cell 101, 451–454.

Nichols, J.T., Miyamoto, A., Olsen, S.L., D'Souza, B., Yao, C., Weinmaster, G., 2007. DSL ligand endocytosis physically dissociates Notch1 heterodimers before activating proteolysis can occur. J. Cell Biol. 176, 445–458.

Opherk, C., Duering, M., Peters, N., Karpinska, A., Rosner, S., Schneider, E., Bader, B., Giese, A., Dichgans, M., 2009. CADASIL mutations enhance spontaneous multimerization of NOTCH3. Hum. Mol. Genet. 18, 2761–2767.

Pratt, E.B., Wentzell, J.S., Maxson, J.E., Courter, L., Hazelett, D., Christian, J.L., 2011. The cell giveth and the cell taketh away: an overview of Notch pathway activation by endocytic trafficking of ligands and receptors. Acta Histochem. 113, 248–255.

Ruchoux, M.M., Chabriat, H., Bousser, M.G., Baudrimont, M., Tournier-Lasserve, E., 1994. Presence of ultrastructural arterial lesions in muscle and skin vessels of patients with CADASIL. Stroke 25, 2291–2292.

Shawber, C.J., Kitajewski, J., 2004. Notch function in the vasculature: insights from zebrafish, mouse and man. Bioessays 225–234.

Takahashi, K., Adachi, K., Yoshizaki, K., Kunimoto, S., Kalaria, R.N., Watanabe, A., 2010. Mutations in NOTCH3 cause the formation and retention of aggregates in the endoplasmic reticulum, leading to impaired cell proliferation. Hum. Mol. Genet. 19, 79–89.

Please cite this article as: Watanabe-Hosomi, A., et al., Transendocytosis is impaired in CADASIL-mutant NOTCH3, Exp. Neurol. (2011), doi:10.1016/j.expneurol.2011.10.020

Journal of the Neurological Sciences 318 (2012) 115–118

Contents lists available at SciVerse ScienceDirect

Journal of the Neurological Sciences

journal homepage: www.elsevier.com/locate/jns

Hereditary diffuse leukoencephalopathy with axonal spheroids caused by R782H mutation in *CSF1R*: Case report

Michiaki Kinoshita [a], Kunihiro Yoshida [b], Kiyomitsu Oyanagi [b], Takao Hashimoto [c], Shu-ichi Ikeda [a,*]

[a] Department of Medicine (Neurology and Rheumatology), Shinshu University School of Medicine, Matsumoto 390-8621, Japan
[b] Department of Brain Disease Research, Shinshu University School of Medicine, Matsumoto 390-8621, Japan
[c] Department of Neurology, Aizawa Hospital, Matsumoto 390-8510, Japan

ARTICLE INFO

Article history:
Received 29 February 2012
Accepted 15 March 2012
Available online 14 April 2012

Keywords:
Dementia
Leukoencephalopathy
CADASIL
Neuroaxonal spheroids
Colony stimulating factor 1 receptor

ABSTRACT

We report a biopsy-proven and genetically determined case with leukoencephalopathy showing autosomal dominant inheritance and pre-senile dementia. A 51-year old woman gradually developed a decline in cognitive functions with aphasia and epileptic seizures. Four of her family members were diagnosed as having dementia in their forties to sixties. Five years later she became apathetic and bed-ridden. Brain MRI initially showed fronto-temporal dominant cerebral atrophy with multiple small lacunar-like lesions in the deep white matter, but these white matter lesions became diffuse at an advanced stage. Such possibilities as hereditary vascular or fronto-temporal dementia were clinically suspected, but her family members requested a definitive diagnosis. Brain biopsy showed severe loss of myelin and axons in the white matter with relatively preserved cortical structure. The remaining axons disclosed irregular shapes with the formation of many spheroids, and these findings were consistent with a histopathological diagnosis of neuroaxonal dystrophy. DNA analysis disclosed a novel heterozygous c.2345 G>A (p.782Arg>His) mutation in exon 18 of the colony stimulating factor 1 receptor gene (*CSF1R*). Hereditary diffuse leukoencephalopathy with axonal spheroids should be included in the differential diagnosis of familial occurrence of pre-senile dementia.

1. Introduction

Leukoencephalopathy or leukodystrophy is characterized pathologically by extensive degenerative and/or demyelinating lesions in cerebral white matter and produces various clinical manifestations such as behavioral and/or mood changes, dementia, motor impairment and epilepsy [1]. The hereditary form of this disorder is rare, but recent advances in diagnostic techniques have made it possible to make a correct pre-mortem diagnosis for some diseases including cerebral autosomal dominant or autosomal recessive arteriopathy with subcortical ischemic leukoencephalopathy (CADASIL [2,3] or CARASIL [4,5]). Recently, another unique form of the disease, hereditary diffuse leukoencephalopathy with axonal spheroids (HDLS) [6], has been noted. To date, more than 20 families have been reported with HDLS [7,8] or familial pigmentary orthochromatic leukodystrophy (POLD) [9,10], both of which are now regarded as a single disease entity because of their clinical and pathological similarities [8,11]. Rademakers et al. [12] have just reported that HDLS is caused by mutations in the colony stimulating factor 1 receptor gene (*CSF1R*). We here describe an HDLS case with a novel mutation in *CSF1R*.

2. Case report

A 51-year-old woman was admitted to our hospital because of gradual cognitive decline. At first she had difficulty in doing simple calculations and driving a car, and had to quit her job. Then her daily activities including house-keeping works became clumsy. On admission, attention and verbal fluency were remarkably disturbed and her score on a Mini Mental State Examination (MMSE) was 20/30 points. MRI showed fronto-temporal atrophy with hyperintense multiple small lesions in the deep cerebral white matter (Fig. 1a, b and c), and she was thus thought to have some form of vascular dementia, although she had no hypertension, hyperlipidemia or diabetes mellitus. Thereafter, her neuropsychiatric and neurological symptoms rapidly progressed, and she fell into an apathetic state with frequent epileptic seizures. When we re-examined her at age 56, she showed mutism, forced grasping, snout and palmomental reflexes, and spastic tetraparesis with hyperactive deep tendon reflexes. MRI revealed progression of brain atrophy with diffuse white matter lesions (Fig. 1d, e and f). It was reported that four other family members were affected by a similar disorder, indicating an autosomal dominant inheritance (Fig. 2). Her husband and daughter desired a definitive diagnosis for possible treatment and/or prevention of disease progression, so after obtaining informed consent from family members and approval from the local ethics committee, a brain biopsy was performed in the right frontal lobe.

* Corresponding author at: Department of Medicine (Neurology and Rheumatology), Shinshu University School of Medicine, Matsumoto 390-8621, Japan. Tel.: +81 263 37 2671; fax: +81 263 37 3427.
E-mail address: ikedasi@shinshu-u.ac.jp (S. Ikeda).

0022-510X/$ – see front matter © 2012 Elsevier B.V. All rights reserved.
doi:10.1016/j.jns.2012.03.012

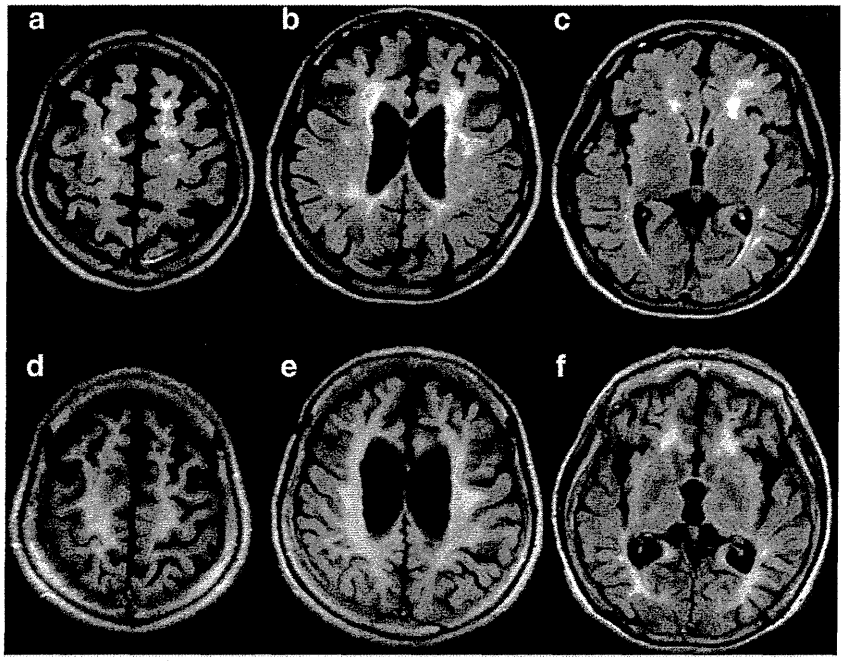

Fig. 1. Serial MRI flair images. The first examination showed multiple small lacuna-like lesions in deep white matter (a, b and c), but in the second examination (d, e and f) these small lesions had become confluent, revealing extensive high signal intensity areas in cerebral white matter.

3. Neuropathological findings

Two small pieces of brain tissue were processed for routine histological, immunohistochemical and electron-microscopic examinations. Microscopically, widespread loss of myelinated fibers was seen in the white matter (Fig. 3a and b) where remaining axons showed irregularly shaped spheroids: these spheroids were clearly seen with hematoxylin and eosin (H&E) and Bodian staining (Fig. 3c), and were also slightly positively stained by periodic acid Schiff (PAS). They were immunopositive for phosphorylated neurofilament (Fig. 3d), but there were few pigmented macrophages. Electron microscopy of axonal spheroids showed numerous degenerative structures such as dense bodies (Fig. 4a), lamellar structures (Fig. 4b) and roughly arranged filaments. There was no conspicuous change in the cerebral cortex including vascular structures.

4. DNA analysis

We extracted genomic DNA from her peripheral blood leukocytes using Gentra Puregene Blood Kit (Qiagen), and exons 12–22 of the *CSF1R* were amplified by polymerase chain reaction (PCR). Direct sequence analysis of the PCR-amplified DNA revealed a novel heterozygous c.2345 G>A (p.782Arg>His) mutation in exon 18 (Fig. 5a). This mutation was not found in 80 Japanese control individuals.

5. Discussion

The clinical picture of HDLS is as follows [11,13]: age of onset ranging from 8 to 78 years (average: 39 years), autosomal dominant inheritance, and dementia with leukoencephalopathy. Neuropsychiatric symptoms including depression, anxiety, behavioral changes

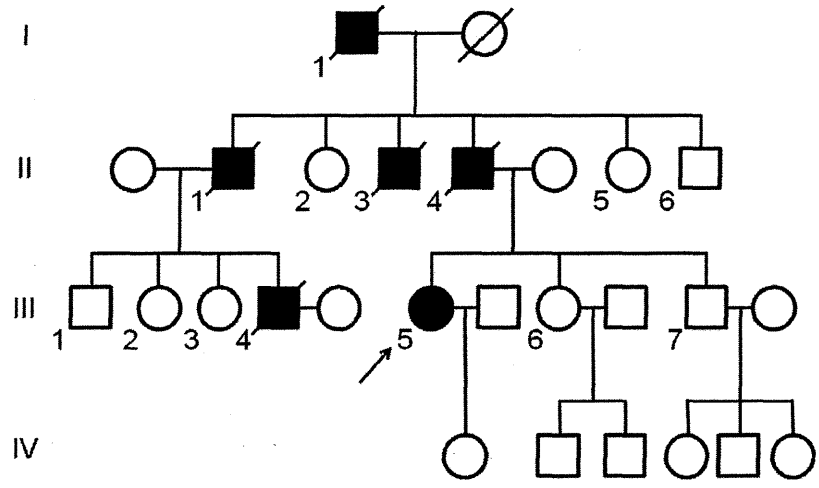

Fig. 2. Family pedigree. An arrow indicates the proband (the present patient). I-1: Her grandfather developed dementia in his seventies and died at the age of 73. II-1, 3 and 4: they started to suffer from progressive cognitive decline in their fifties and sixties, and died in their seventies. III-4: Her cousin developed dementia in his forties and died at the age of 55.

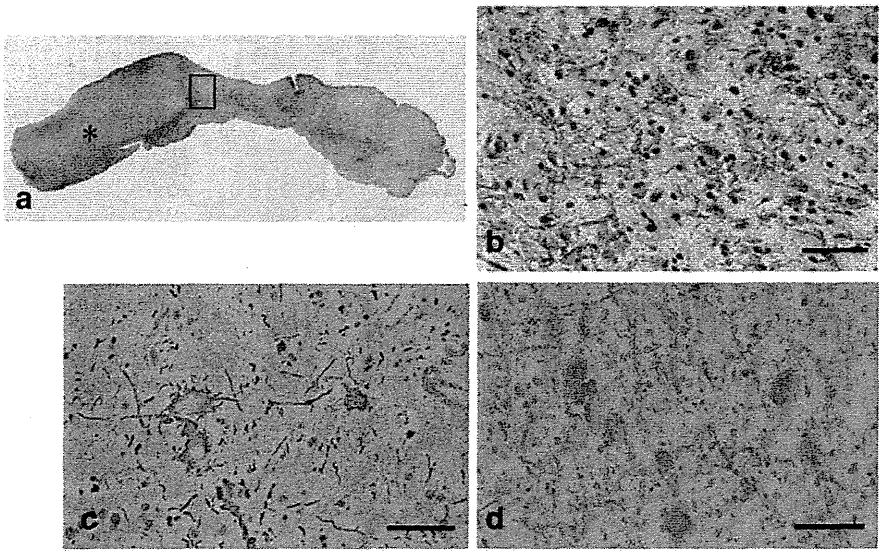

Fig. 3. Neuropathological and immunohistochemical findings of the biopsied specimen. Severe loss of myelinated fibers is seen in the cerebral white matter (a and b). (Klüver–Barrera stain, b: higher magnification of the framed area in a) (bar in b = 50 μm). The asterisk in a indicates cerebral cortex. The number of axons is reduced and there are large spheroids 20 to 50 μm in diameter (c) (Bodian stain, bar = 50 μm). These spheroids are positively immunolabeled by an anti-phosphorylated neurofilament (d) (SMI-31, Sternberger Monoclonals, Baltimore, MD, ×2000) (immunoperoxidase staining, bar = 50 μm).

and cognitive disturbance usually precede neurological manifestations, with the latter consisting of spastic paresis, parkinsonism, ataxia, and epilepsy. Clinical manifestations in our patient were very similar to those of the previously reported patients with HDLS [11,13], and she was definitively diagnosed by brain biopsy. It is supposed that the cerebral white matter lesions start in the frontal lobes and/or corpus callosum and that the earliest lesions are multifocal [9,14]. The initial MRI of our patient confirmed the presence of multifocal small lesions in the deep white matter, indicating that she was affected by vascular dementia. However, subsequent MRI examinations disclosed that these small lesions became confluent during the progression of the disease, ultimately producing extensive white matter lesions with predominant involvement of the frontal and temporal lobes. The serial neuroimages of our patient were therefore useful in understanding the disease progression of HDLS.

Although the disease concept of HDLS had been established, the underlying genetic background remained unclear. Very recently, 14 different mutations in *CSF1R* were identified in 14 families with HDLS and all were located in exons 12–22, encoding the intracellular tyrosine kinase domain of CSF1R protein [12], indicating that CSF1R-dependent abnormal phosphorylation of tyrosine residues is a key event in the development of HDLS. Indeed, a transient expression study in cultured HeLa cells has shown that autophosphorylation on multiple tyrosine residues is disturbed in several mutant CSF1R proteins [12]. The p.R782H identified in our patient is also located in the tyrosine kinase domain and p.R782 is strongly conserved between species and within members of the CSF1/platelet-derived growth factor (PDGF) family of tyrosine kinase (Fig. 5b). In silico analysis using PolyPhen-2 indicated that the change was probably damaging. It is, therefore, very likely that p.R782H is a disease-causing mutation in our patient.

One of the pathologic hallmarks of HDLS is the presence of numerous neuroaxonal spheroids in cerebral white matter. However, it is still controversial whether the spheroids are caused by primary axonal damage or not [11]. CSF1R is mainly expressed in microglial cells in the brain, and is involved in the regulation, survival, proliferation and differentiation of microglial cells [12]. Therefore, the molecular process of microglial dysfunction to spheroid formation needs further investigation to clarify the pathogenesis of HDLS.

Finally, an ante-mortem diagnosis of HDLS is quite difficult because of the limitation of diagnostic approaches. As a result, HDLS patients have been often misdiagnosed with CADASIL, fronto-temporal dementia, motor neuron disease with dementia, multiple sclerosis, or Binswanger disease [11]. In particular, the differentiation of HDLS from CADASIL seems to be rather difficult on the basis of clinical pictures and neuroimages [13,15]. Molecular analysis of *CSF1R* is, therefore,

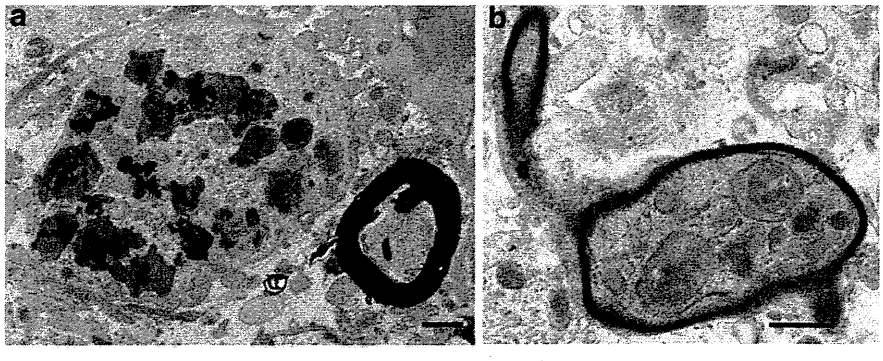

Fig. 4. Electron micrographs of spheroids. A swollen axon is packed with degenerative structures, such as dense bodies (a). Another swollen axon contains myelin-figure structures (b) (bars = 1.5 μm).

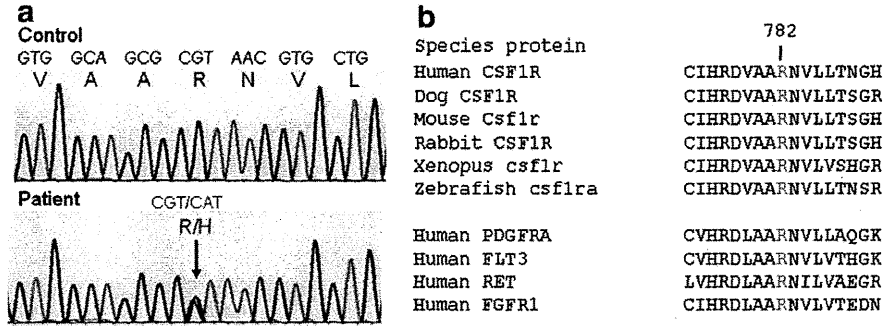

Fig. 5. Molecular analysis of *CSF1R*. Sequencing result of exon 18 of *CSF1R* indicates a heterozygous c.2345 G>A (p.782Arg>His) substitution in the patient (a). cDNA and protein numberings are relative to NM_005211.3 starting at the translation initiation codon and NP_005202.2, respectively. The comparison of amino acid alignment around p.782R in the protein tyrosine kinase domain between human CSF1R and several CSF1R orthologues and human CSF1/PDGF receptor paralogues is shown (b). The p.782R is completely conserved among CSF1R orthologues and CSF1/PDGF receptor paralogues. Data are based on Protein ID (Ensembl genome browser 65, available at http://asia.ensembl.org/); they are as follows: human CSF1R (*ENSP00000286301*), dog CSF1R (*ENSCAFP00000026920*), mouse Csf1r (*ENSMUSP00000025523*), rabbit CSF1R (*ENSOCUP00000020310*), Xenopus csf1r (ENSXETP00000061910), zebrafish csf1ra (ENSDARP00000089365), human PDGFRA (ENSP00000257290), human FLT3 (ENSP00000241453), human RET (ENSP00000347942), and human FGFR1 (ENSP00000380280).

very valuable for differential diagnosis in patients with familial adult-onset dementia with prominent white matter lesions in brain imaging.

Ethics approval

This study was conducted with the approval of the Ethical Committee of Shinshu University School of Medicine.

Acknowledgments

We thank Dr. Tatsuya Kobayashi, Department of Neurosurgery, Shinshu University School of Medicine, for providing us with brain biopsy specimens, and Prof. Osamu Onodera, Center for Bioresource-based Researches, Brain Research Institute, Niigata University, for his useful comments on this manuscript.

References

[1] Powers JM. A neuropathologic overview of the neurodystrophies and neurolipidoses. In: Vinken PJ, Bruyn GW, editors. Handbook of Clinical Neurology, vol. 66. Amsterdam: Elsevier; 1996. p. 1–32.
[2] Joutel A, Corpechot C, Ducros A, Vahedi K, Chabriat H, Mouton P, et al. Notch 3 mutations in CADASIL, a hereditary adult-onset condition causing stroke and dementia. Nature 1996;383:707–10.
[3] Rucoux MM, Maurage CA. CADASIL: cerebral autosomal dominant arteriopathy with subcortical infarcts and leukoencephalopathy. J Neuropathol Exp Neurol 1997;56:947–64.
[4] Yanagawa S, Ito N, Arima K, Ikeda S. Cerebral autosomal recessive arteriopathy with subcortical infarcts and leukoencephalopathy. Neurology 2002;58:817–20.
[5] Hara K, Shiga A, Fukutake T, Nozaki H, Miyashita A, Yokoseki A, et al. Association of HTRA1 mutations and familial ischemic cerebral small-vessel disease. N Engl J Med 2009;360:1729–39.
[6] Axelsson R, Röyttä M, Sourander P, Akesson HO, Andersen O. Hereditary diffuse leukoencephalopathy with spheroids. Acta Psychiatr Scand Suppl 1984;314:1–65.
[7] Terada S, Ishizu H, Yokota O, Ishihara T, Nakashima H, Kugo A, et al. An autopsy case of hereditary diffuse leukoencephalopahty with spheroids, clinically suspected of Alzheimer's disease. Acta Neuropathol 2004;108:538–45.
[8] Marotti JD, Tobias S, Fratkin JD, Powers JM, Rohdes CH. Adult onset leukodystrophy with neuroaxonal spheroids and pigmented glia: report of a family, historical perspective, and review of the literature. Acta Neuropathol (Berl) 2004;107:481–8.
[9] Itoh K, Shiga K, Shimizu K, Muranishi M, Nakagawa M, Fushiki S. Autosomal dominant leukodystrophy with axonal spheroids and pigmented glia: clinical and neuropathological characteristics. Acta Neuropathol 2006;111:39–45.
[10] Ali ZS, Van Der Voorn JP, Powers JM. A comparative morphologic analysis of adult onset leukodystrophy with neuroaxonal spheroids and pigmented glia—a role for oxidative damage. J Neuropathol Exp Neurol 2007;66:660–72.
[11] Wider C, Van Gerpen JA, DeArmond S, Shuster EA, Dickson DW, Wszolek ZK. Leukoencephalopathy with spheroids (HDLS) and pigmentary leukodystrophy (POLD). A single entity? Neurology 2009;72:1953–9.
[12] Rademakers R, Baker M, Nicholson AM, Rutherford NJ, Finch N, Soto-Ortolaza A, et al. Mutations in the colony stimulating factor 1 receptor (*CSF1R*) gene cause hereditary diffuse leukoencephalopathy with spheroids. Nat Genet 2012;44:200–7.
[13] Freeman SH, Hyman BT, Sims KB, Hedley-Whyte ET, Vossough A, Frosch MP, et al. Adult onset leukodystrophy with neuroaxonal spheroids: clinical, neuroimaging and neuropathologic observations. Brain Pathol 2009;19:39–47.
[14] van der Knaap MS, Naidu S, Kleinschmidt-DeMasters BK, Kamphorst W, Weinstein HC. Autosomal dominant diffuse leukoencephalopathy with neuroaxonal spheroids. Neurology 2000;54:463–8.
[15] O'Sullivan M, Jarosz JM, Martin RJ, Deasy N, Powell JF, Markus HS. MRI hyperintensities of the temporal lobe and external capsule in patients with CADASIL. Neurology 2001;56:628–34.

Original Paper

Cerebrovascular Diseases

Cerebrovasc Dis 2012;33:128–134
DOI: 10.1159/000334185

Received: May 10, 2011
Accepted: September 16, 2011
Published online: December 14, 2011

Simultaneous Impairment of Intracranial and Peripheral Artery Vasoreactivity in CADASIL Patients

Yasuhiro Fujiwara[a] Toshiki Mizuno[a] Chio Okuyama[b] Yoshinari Nagakane[a]
Akiko Watanabe-Hosomi[a] Masaki Kondo[a] Nagato Kuriyama[a]
Takahiko Tokuda[a] Shigenori Matsushima[b] Tsunehiko Nishimura[b]
Masanori Nakagawa[a]

Departments of [a]Neurology and [b]Radiology, Kyoto Prefectural University of Medicine, Kyoto, Japan

Key Words
CADASIL · Vasoreactivity · ^{123}I-IMP-SPECT · Reactive hyperemia peripheral arterial tonometry

Abstract
Background: Reduced cerebrovascular reactivity (CVR) is an important step in the pathogenesis of cerebral autosomal dominant arteriopathy with subcortical infarcts and leukoencephalopathy (CADASIL). The present study utilized quantitative single photon emission computed tomography (SPECT) with the autoradiographic (ARG) method and reactive hyperemia peripheral arterial tonometry (RH-PAT) to assess vasoreactivity in intracranial arteries and in peripheral arteries in patients with CADASIL. ***Methods:*** Quantitative SPECT studies were conducted in eight patients with CADASIL, while RH-PAT analysis was conducted in eight CADASIL patients and in eight age-matched normal subjects. Quantitative SPECT studies with the ARG method were performed at baseline and after administration of acetazolamide. Regional cerebral blood flow (rCBF) values were measured using stereotactic extraction estimation (SEE) methods. The rCBF of CADASIL patients was averaged in the bilateral frontal, temporal, parietal, and occipital lobes as well as in the limbic system, cerebellar hemisphere, whole cerebral cortex and basal ganglia. The CVR index from acetazolamide stress of intracranial arteries was calculated in each area. Vasoreactivity of peripheral arteries was estimated by the reactive hyperemia index (RHI) measured with a PAT device before and after interruption of arterial flow. ***Results:*** Average RHI after post-deflation was lower in CADASIL patients than in normal subjects. RHI correlated significantly with CVR in all brain areas in CADASIL patients. ***Conclusions:*** Vasoreactivity is reduced in peripheral arteries and in intracranial arteries in patients with CADASIL.

Introduction

Cerebral autosomal dominant arteriopathy with subcortical infarcts and leukoencephalopathy (CADASIL) is a hereditary microangiopathy due to *Notch3* mutation [1], leading to migraines, recurrent cerebral infarction, and vascular dementia. Notch3 is mainly expressed in vascular smooth muscle cells (VSMCs) and is preferentially ex-

KARGER
Fax +41 61 306 12 34
E-Mail karger@karger.ch
www.karger.com

1015–9770/12/0332–0128$38.00/0

Accessible online at:
www.karger.com/ced

Dr. Toshiki Mizuno
Department of Neurology
Kyoto Prefectural University of Medicine
Kajiicho-465, Kamigyo-ku, Kyoto 602-8566 (Japan)
Tel. +81 75 251 5794, E-Mail mizuno@koto.kpu-m.ac.jp

pressed in small arteries of the adult human brain [2]. Histological examination of systemic arteries from patients with CADASIL has revealed thickening of the arterial wall and degeneration of VSMCs [3]. Therefore, degeneration of VSMCs is thought to represent an important step in the pathogenesis of CADASIL [4]. Early reduced cerebrovascular reactivity (CVR) in intracranial arteries, which may be related to dysfunction of VSMCs, has been demonstrated by various modalities, such as magnetic resonance imaging (MRI) bolus tracking methods [5], single photon emission computed tomography (SPECT) [6], transcranial Doppler (TCD) sonography with acetazolamide [7].

Histologic examination of systemic arteries from transgenic (Tg) mice overexpressing mutant human NOTCH3 has revealed the destruction of VSMCs and the accumulation of granular osmiophilic materials around VSMCs, which is a specific diagnostic feature of CADASIL [8]. Systemic arteries from mutant NOTCH3 Tg mice also have reduced vascular reactivity in response to physiological stimuli [9]. Human pathological studies of skin arteries and cerebral arteries from CADASIL patients have also revealed destruction of VSMCs and the accumulation of granular osmiophilic materials [10]. Although the disease pathology affects mainly the tunica media, endothelial changes and dysfunction have been also reported [11–13]. Moreover, a recent large prospective cohort study showed that atherosclerosis has an impact, although small, on the clinical and brain MRI in CADASIL patients [14]. Ultrasound [12] and laser Doppler techniques [15] have demonstrated that flow-mediated vasodilation (FMD) of the brachial artery is reduced in peripheral vessels in CADASIL patients. Endothelial dysfunction in cerebral vessels has also been shown using the TCD method with L-arginine [13]. However, intracranial and peripheral vasoreactivity have not been compared within the same CADASIL patient, and the relationship between intracranial vasoreactivity and peripheral vasoreactivity in CADASIL patients remains unknown.

Reactive hyperemia peripheral arterial tonometry (RH-PAT) is a novel noninvasive technique to assess peripheral microvascular endothelial function by measuring changes in digital pulse volume during reactive hyperemia [16]. RH-PAT can assess peripheral vasoreactivity more accurately and more easily than FMD [17, 18]. In addition, while brachial artery flow-mediated dilation measures single conduit artery vasodilatation, the PAT hyperemic response largely reflects vasodilatation in digital microvessels.

We hypothesize that the vasoreactivity of intracranial arteries and peripheral arteries are reduced in CADASIL patients. To test this hypothesis, the present study utilized quantitative *N*-isopropyl-*p*-^{123}I-iodoamphetamine (^{123}I-IMP) SPECT with the autoradiographic (ARG) method and RH-PAT to assess vasoreactivity in intracranial arteries and in peripheral arteries in patients with CADASIL.

Materials and Methods

Subjects

Eight CADASIL subjects (three males and five females; mean age 54.6 ± 13.1 years, range 42–75 years) from six families were recruited for this study. All CADASIL patients were diagnosed with CADASIL according to clinical symptoms, imaging studies and detection of a *Notch3* mutation. Eight aged-matched normal subjects (five males and three females; mean age 48.9 ± 5.3 years, range 40–57 years) were recruited for PAT analysis. Mini-mental state examination (MMSE) and modified Rankin Scale (mRS) were evaluated in all CADASIL patients.

Image Acquisition and Analysis

MRI was performed at the time of the study using a 1.5T MR instrument (Gyroscan Intera Nova; Philips Medical Systems, Best, The Netherlands). The severity of white-matter lesions (WML) on a fluid-attenuated inversion recovery (FLAIR) image was classified into four different grades, as previously reported [19].

Two quantitative SPECT studies with the ARG method were performed within a 7-day period. The first study was performed as a baseline study, and the second study was performed following acetazolamide injection on a separate day from the first study. For both studies, a 185 MBq dose of ^{123}I-IMP (Nihon Mediphysics, Hyogo, Japan) was injected intravenously with the subject at rest in a sitting position with the eyes open. Measurement of regional cerebral blood flow (rCBF) was performed in accordance with the ARG method, as previously reported [20]. One-point arterial blood sampling was performed from the brachial artery at 10 min after the start of ^{123}I-IMP injection for the assessment of whole blood radioactivity concentration. SPECT examination was started 22 min after the intravenous ^{123}I-IMP injection and was conducted for 16 min using a triple-head gamma camera system (PRISM IRIX; Picker International, Cleveland, Ohio, USA) equipped with low energy, parallel collimators. The SPECT images with a 128 × 128 matrix were reconstructed using ordered-subset expectation maximization (OSEM) reconstructions with four iterations and 12 subsets. Attenuation correction was performed using Chang's method, and scatter was corrected with the triple-energy window method. For the acetazolamide stress study, acetazolamide (1 g) was administered intravenously starting 10 min before the beginning of ^{123}I-IMP injection. For each subject, data obtained from ^{123}I-IMP SPECT images were analyzed with three-dimensional stereotactic surface projections (3D-SSP) using image-analysis software (iSSP version 5, Nihon Mediphysics, Hyogo, Japan), which was modified based on the NEUROSTAT program [21, 22], and data were normalized to the mean global activity. Stereotactic extraction (SEE) estimation was conducted with

Table 1. Clinical data from eight CADASIL patients

Case	Age	Gender	Notch3 mutation	MMSE score	mRS	Severity of MRI WML
1	49	Female	R182C	30	0	C
2	42	Female	R332C	24	3	D
3	68	Female	R141C	20	4	D
4	47	Male	R141C	30	0	D
5	45	Male	C106R	29	0	C
6	67	Female	C106R	22	0	D
7	45	Female	R141C	24	0	C
8	75	Male	R141C	22	4	D

Severity of WML in the FLAIR imaging was classified by Chabriat's method [15].

Table 2. rCBFs before and after acetazolamide injection, and rCVRs in the cerebral whole cortex and in each brain area in patients with CADASIL

	rCBF at rest ml/100 g/min	rCBF after ACZ injection ml/100 g/min	rCVR %
Frontal	37.7 ± 6.4	63.8 ± 11.4	74.6 ± 47.6
Temporal	35.4 ± 6.8	61.3 ± 11.1	79.9 ± 52.7
Parietal	41.1 ± 8.1	68.3 ± 12.6	72.1 ± 49.3
Occipital	45.7 ± 10.6	73.3 ± 10.4	69.3 ± 51.7
Limbic	37.0 ± 7.0	61.0 ± 8.9	71.3 ± 46.2
Cerebellar	43.4 ± 12.0	64.3 ± 10.1	56.1 ± 42.1
Whole cortex	38.4 ± 7.0	64.3 ± 10.6	73.1 ± 48.0
Brain stem	34.1 ± 7.4	51.7 ± 7.7	56.9 ± 38.7

analysis software (SEE version 2.1, Nihon Mediphysics, Hyogo, Japan) to quantify rCBF in each area. The accuracy of rCBF values obtained by this technique in combination with ARG methods is supported by a previous study, which documented the utility of SEE and 3D-SSP programs with ARG methods to objectively assess the severity of hemodynamic brain ischemia [23]. The whole brain was divided into segments according to SEE methods (level 1; cerebrum, cerebellum, brainstem, level 2; lobe level classification), and the rCBF values (ml/100 g/min) of CADASIL patients were averaged in the bilateral frontal, temporal, parietal, and occipital lobes as well as in the limbic system, cerebellar cortex, whole cerebral cortex and brainstem. CVR index from acetazolamide stress of intracranial arteries was calculated as follows:

rCVR (%) = ([acetazolamide challenge rCBF – resting rCBF]/resting rCBF) × 100.

Endothelium-Dependent FMD

To investigate endothelial vasomotor function using RH-PAT, digital pulse amplitude was measured with a PAT device placed on the tip of each finger (Endo-PAT 2000; Itamar Medical, Caesarea, Israel). After baseline pulse amplitude was measured for 5 min, arterial flow was interrupted for 5 min by placing a cuff on the left proximal forearm at 200 mm Hg occlusion pressure. After releasing the pressure, pulse amplitude was recorded electronically in bilateral fingers and was analyzed with a computerized automated algorithm. Reactive hyperemia index (RHI) of peripheral arteries was calculated as follows:

RHI = (test/baseline ratio of test arm)/(test/baseline ratio of control arm) × baseline correction factor.

The augmentation index was defined as the ratio of height of the peak above the shoulder of the wave to the pulse pressure. It was calculated automatically by analyzing the waveform of the PAT signal, averaged from multiple signals during the baseline period. Peripheral pulsation was intact, and arteriosclerosis obliterans was excluded in these subjects.

This study protocol was approved by the ethical committee of Kyoto Prefectural University. Written informed consent was obtained from all subjects.

Statistical Analysis

Data are expressed as mean ± SD. Regional CBF before and after acetazolamide injections were compared using the paired t test. Regional CBF before or after acetazolamide injection and CVR in each area were compared among CADASIL patients using the analysis of variance (ANOVA) test. RHI was compared between CADASIL and normal subjects using the Mann-Whitney test. Correlations between CVR and RHI were determined by the Piason test. A p value <0.05 was considered to represent statistical significance. Statistical analyses were performed with Dr. SPSS II for Windows (SPSS Japan Inc., Tokyo, Japan).

Results

Clinical Data

The clinical characteristics of eight CADASIL patients are summarized in table 1. mRS ranged from 0 to 4 (0 in five patients, 3 in one patient, and 4 in two patients). MMSE score ranged from 20 to 30. Three patients (cases 1, 5, 7) had nodular or moderate periventricular hyperintensities on FLAIR images (score C), while five patients (cases 2, 3, 4, 6, 8) had confluent lesions or severe periventricular hyperintensities (score D). WMLs in the anterior part of the temporal lobes, which are typical MRI findings in CADASIL, were observed in six patients (cases 1, 3, 4, 6, 7, 8).

SPECT Study

Table 2 summarizes rCBFs before and after acetazolamide injection and rCVRs in each brain area in CADASIL patients. The averaged rCBFs before and after acetazolamide injection were comparatively lower in the temporal lobe and limbic system than in the occipital lobe, but the averaged rCBFs before or after acetazol-

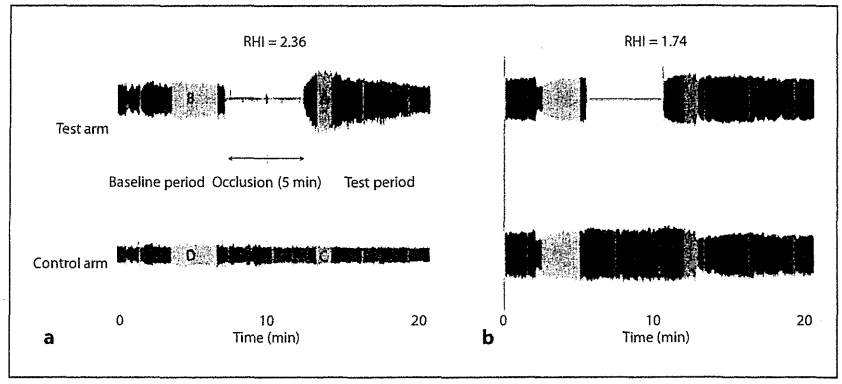

Fig. 1. Representative pulse amplitude tracing in CADASIL patients (**b**) and in normal subjects (**a**). The x- and y-axes represent time and pulse volume amplitude, respectively. Sequential pulse amplitude of the bilateral second fingers was recorded before and after interrupting arterial flow for 5 min using a cuff placed on the forearm. Each gray area represents a region of interest for the automated calculation. RHI was calculated as follows: RHI = (A/B)/(C/D) × baseline correction factor. RHI was lower in CADASIL patients than in normal subjects.

amide injection did not differ significantly among different brain areas. The averaged rCBF values of the whole cerebral cortex were significantly higher after acetazolamide injection (64.3 ± 10.6 ml/100 g/min) than before acetazolamide injection (38.4 ± 7.0 ml/100 g/min). The rCBF in each cerebral cortex significantly increased after acetazolamide injection, and the minimum value of rCVR was 69.3 ± 51.7% in the occipital lobe while the maximum value was 79.9 ± 52.7% in the temporal lobe.

Post-Occlusive Hyperemic Test (Endo-PAT 2000)

Representative pulse amplitude tracing in CADASIL and control patients is illustrated in figure 1. In the control patients, the pulse amplitude rose rapidly after forearm cuff deflation in the hyperemic fingertip, with maximal response occurring in the 60- to 90-s postdeflation interval. In the contralateral arm, only minimal increase or no increase was seen after deflation. Averaged RHI was significantly lower in CADASIL patients (1.49 ± 0.17) than in normal subjects (2.18 ± 0.62; p = 0.01) (fig. 2; table 3). These results suggest that the postdeflation hyperemic response in peripheral arteries was abnormal in CADASIL patients.

There were no significant differences between the CADASIL patients and normal subjects in terms of age, systolic and diastolic blood pressure, or laboratory test results (table 3). The relationship between CVR from SPECT study and RHI from RH-PAT was assessed (fig. 3) and demonstrated a significant correlation between averaged CVR in the whole cortex and RHI (r = 0.872, p = 0.005). There was also a significant correlation between CVR in any area of the brain and RHI (frontal, parietal, temporal, and occipital lobes and limbic system, cerebellar cortex and brainstem, r = 0.823, 0.842, 0.887, 0.896, 0.910, 0.895,

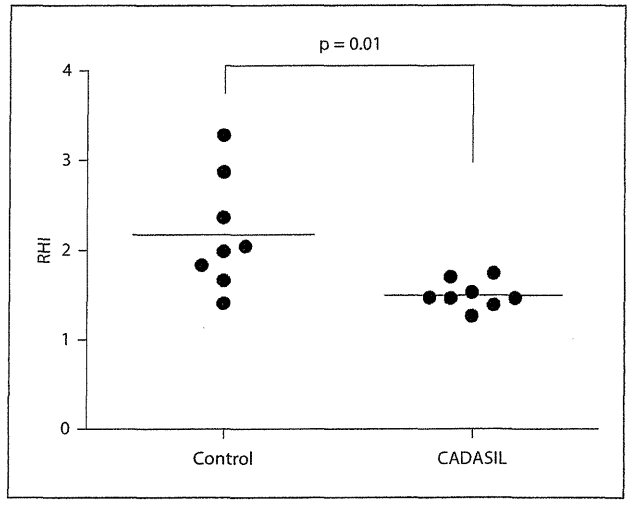

Fig. 2. Scatter plot of RHI in CADASIL patients and in normal subjects. Averaged RHI was significantly lower in eight CADASIL patients than in eight normal subjects (1.49 ± 0.17 vs. 2.18 ± 0.62, respectively).

Table 3. Clinical characteristics and indices from PAT analysis of CADASIL patients and normal subjects

Characteristic	CADASIL (n = 8)	Control (n = 8)	p value
Age, years	54.6 ± 13.1	48.9 ± 5.3	NS
Men/women	3/5	5/3	NS
Systolic BP, mm Hg	117.6 ± 11.4	120.0 ± 10.1	NS
Diastolic BP, mm Hg	71.6 ± 10.5	80.0 ± 9.5	NS
RHI	1.49 ± 0.17	2.18 ± 0.62	0.01
Augmentation index	8.14 ± 16.21	10.86 ± 25.73	NS

BP = Blood pressure; NS = not significant.

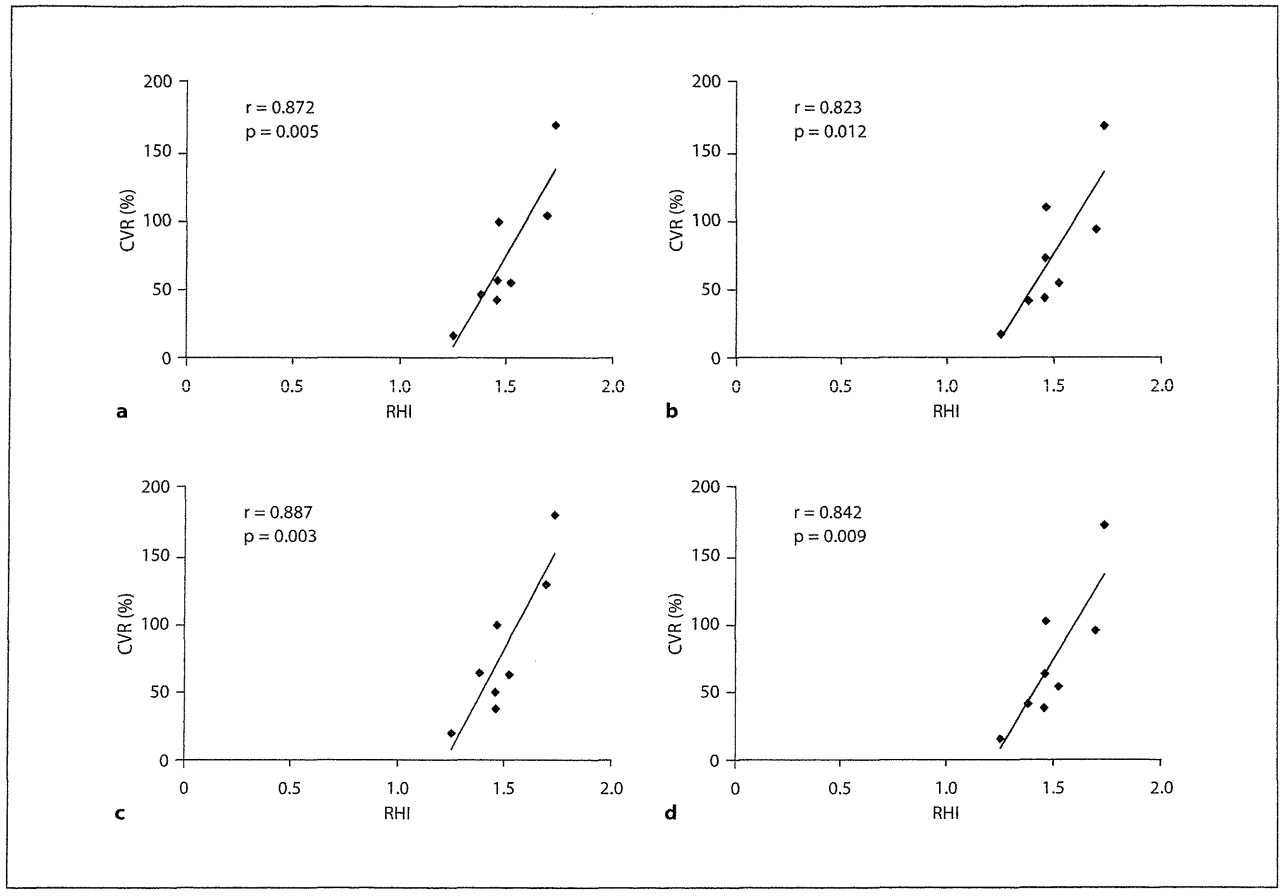

Fig. 3. Correlation between CVR and RHI of the whole cortex (**a**), frontal cortex (**b**), temporal cortex (**c**), and parietal cortex (**d**). CVRs in the whole cortex and each cortex correlated with RHI.

and 0.901, respectively; p = 0.012, 0.009, 0.003, 0.003, 0.002, 0.003, and 0.002, respectively). In contrast, there was no correlation between RHI and MMSE, RHI and mRS, CVR and MMSE, CVR and mRS.

Discussion

The present study used IMP-ARG and RH-PAT to demonstrate that vasoreactivity was reduced in both peripheral arteries and in intracranial arteries in patients with CADASIL. Among the various findings, this study showed that the hyperemic response after postdeflation was lower in CADASIL patients than in normal control subjects. Previous studies have documented the utility of Endo-PAT in the assessment of peripheral vasomotor function [16]. Digital hyperemic response as measured by Endo-PAT may be induced by production of nitric oxide (NO) during occlusion of peripheral artery, since previous studies demonstrated that an endothelial NO synthase inhibitor blunted the increase in digital pulse volume amplitude during reactive hyperemia [24]. The reduction of average RH-PAT index in patients with coronary endothelial dysfunction [25] and the strong relationship between the PAT ratio and multiple vascular risk factors [26] suggests that RH-PAT can accurately detect endothelial dysfunction and assess peripheral vasomotor function. In CADASIL patients, altered endothelial-dependent vasodilatation in cerebral and forearm arteries and higher levels of asymmetrical dimethylarginine, a NO endogenous inhibitor, have been found [12, 13, 27]. These data, in combination with other studies show-

ing a pathological change in VSMCs and endothelial cells in patients with CADASIL, suggest that the reduction of the reactive hyperemic response may be mediated by abnormalities in NO-induced relaxation of VSMCs in patients with CADASIL.

Previous reports using venous occlusive plethysmography demonstrated a reduction of forearm blood flow in CADASIL patients, possibly because of impaired endothelium-dependent vasodilation in resistance arteries. By contrast, the FMD and the pulse wave method did not show any reduction in endothelium-dependent vasodilation in conduit arteries [12]. Further, Gobron et al. [15] reported no alteration in the post-occlusive hyperemic response of CADASIL patients when using a laser Doppler flow meter attached to the finger. However, the delayed response of time to peak and whole duration time in the post-occlusive hyperemia was much larger in CADASIL patients than in normal control subjects. In comparison to ultrasound or laser Doppler techniques, RH-PAT has the advantage of being able to evaluate vascular tone in the peripheral arterial beds quantitatively and accurately after occlusive hyperemia, because the PAT biosensor imparts a uniform sub-diastolic pressure field and because simultaneous recording can exclude the systemic vascular response. Indeed, use of this technique in the present study allowed the characterization of abnormalities in peripheral vasoreactivity in CADASIL patients.

Brulin et al. [28] showed that marked destruction of smooth muscle cells in skin vessels and in brain vessels in patients with CADASIL resulted in a decrease of vessel wall thickness and loss of extracellular matrix area, thereby contributing to vessel wall weakness and hypotonicity of the central and peripheral arteries. These and other findings support the notion that there is dysfunction of arterial tone in the central and peripheral arteries in humans as well as in Tg animals with CADASIL [9, 29]. Indeed, the significant correlation between CVR and RH-PAT in the present study suggested dysfunction in both the cerebral and peripheral arteries in CADASIL patients and that assessment of central vascular function may be more easily (although indirectly) assessed through characterization of peripheral vascular function in patients with CADASIL.

The present study has several limitations. First, the number of CADASIL patients included in the present study was small, which precluded comprehensive statistical analysis. Second, the spatial resolution and quantification of rCBF using the SPECT scanner was low when compared with positron emission tomography (PET), particularly when employed in the white matter. To improve quantitative evaluation in SPECT study, the present study applied IMP-SPECT with the ARG and the SEE method. Previous studies have demonstrated that rCBF measurements with the IMP-SPECT method correlated well with that obtained by PET [20]. Further, the SEE method of quantifying rCBF within different brain regions can obviate the technical issues or bias associated with arbitrary selection of a specific brain area [21–23]. Third, different methods were used to evaluate vascular reactivity in intracranial arteries and in peripheral arteries. Specifically, peripheral vasoreactivity was evaluated with RH-PAT induced by hyperemia, while intracranial vasoreactivity was evaluated by SPECT with an acetazolamide challenge. Still, previous studies have reported that the average RH-PAT index significantly correlated with the coronary blood flow response to acetylcholine [25, 30], which suggests that Endo-PAT can accurately assess vasoreactivity regardless of the vascular beds or specific stimulus. In conclusion, the present study demonstrated that the vasoreactivity of peripheral and intracranial arteries is reduced in patients with CADASIL. The correlation between the reduction in peripheral and central vasoreactivity suggests that RH-PAT may be a useful non-invasive strategy to predict intracranial vasoreactivity in patients with CADASIL.

References

1 Joutel A, Corpechot C, Ducros A, Vahedi K, Chabriat H, Mouton P, Alamowitch S, Domenga V, Cecillion M, Marechal E, Maciazek J, Vayssiere C, Cruaud C, Cabanis EA, Ruchoux MM, Weissenbach J, Bach JF, Bousser MG, Tournier-Lasserve E: Notch3 mutations in CADASIL, a hereditary adult-onset condition causing stroke and dementia. Nature 1996;383:707–710.

2 Joutel A, Andreux F, Gaulis S, Domenga V, Cecillon M, Battail N, Piga N, Chapon F, Godfrain C, Tournier-Lasserve E: The ectodomain of the notch3 receptor accumulates within the cerebrovasculature of CADASIL patients. J Clin Invest 2000;105:597–605.

3 Ruchoux MM, Guerouaou D, Vandenhaute B, Pruvo JP, Vermersch P, Leys D: Systemic vascular smooth muscle cell impairment in cerebral autosomal dominant arteriopathy with subcortical infarcts and leukoencephalopathy. Acta Neuropathol (Berl) 1995;89:500–512.